Eur. Phys. J. A (2023) 59:208
https://doi.org/10.1140/epja/s10050-023-01081-w

THE EUROPEAN PHYSICAL JOURNAL A

Regular Article - Experimental Physics

PANDORA Project for the study of photonuclear reactions below $A = 60$

PANDORA Collaboration

A. Tamii[1,2,3,a], L. Pellegri[4,5], P.-A. Söderström[6], D. Allard[7], S. Goriely[8], T. Inakura[9], E. Khan[10], E. Kido[11], M. Kimura[11,12,13], E. Litvinova[14], S. Nagataki[11], P. von Neumann-Cosel[15], N. Pietralla[15], N. Shimizu[16], N. Tsoneva[6], Y. Utsuno[17], S. Adachi[18], P. Adsley[19,20], A. Bahini[5], D. Balabanski[6], B. Baret[7], J. A. C. Bekker[4,5], S. D. Binda[4,5], E. Boicu[6,21], A. Bracco[22,23], I. Brandherm[15], M. Brezeanu[6,21], J. W. Brummer[5], F. Camera[22,23], F. C. L. Crespi[22,23], R. Dalal[24], L. M. Donaldson[5], Y. Fujikawa[25], T. Furuno[3], H. Haoning[14], R. Higuchi[11], Y. Honda[3], A. Gavrilescu[6,26], A. Inoue[1], J. Isaak[15], H. Jivan[4,5], P. Jones[5], S. Jongile[5], O. Just[11,27], T. Kawabata[3], T. Khumalo[4,5], J. Kiener[10], J. Kleemann[15], N. Kobayashi[1], Y. Koshio[28], A. Kuşoğlu[6,29], K. C. W. Li[30], K. L. Malatji[5], R. E. Molaeng[4,5], H. Motoki[12], M. Murata[1], A. A. Netshiya[4,5,31], R. Neveling[5], R. Niina[1], S. Okamoto[25], S. Ota[1], O. Papst[15], E. Parizot[10], T. Petruse[6], M. S. Reen[32], P. Ring[33], K. Sakanashi[3], E. Sideras-Haddad[4], S. Siem[30], M. Spall[15], T. Suda[34], T. Sudo[1], Y. Taniguchi[35], V. Tatischeff[10], H. Utsunomiya[36,37], H. Wang[36,38,39], V. Werner[15], H. Wibowo[40], M. Wiedeking[4,5], O. Wieland[23], Y. Xu[6], Z. H. Yang[41]

[1] Research Center for Nuclear Physics (RCNP), Osaka University, Ibaraki 567-0047, Japan
[2] Institute for Radiation Sciences (IRS), Osaka University, Toyonaka, Osaka 560-0043, Japan
[3] Department of Physics, Osaka University, Toyonaka, Osaka 560-0043, Japan
[4] School of Physics, University of the Witwatersrand, Johannesburg 2050, South Africa
[5] iThemba Laboratory for Accelerator Based Sciences, Somerset West 7129, South Africa
[6] Extreme Light Infrastructure-Nuclear Physics (ELI-NP)/Horia Hulubei National Institute for Physics and Nuclear Engineering (IFIN-HH), Str. Reactorului 30, Bucharest-Măgurele 077125, Romania
[7] Laboratoire Astroparticule et Cosmologie, CNRS, Université Paris Cité, 10 rue ALiceDomon et Léonie Duquet, 75013 Paris, France
[8] Institut d'Astronomie et d'Astrophysique, Université Libre de Bruxelles, Campus de la Plaine, CP 226, 1050 Brussels, Belgium
[9] Tokyo Institute of Technology, 2-12-1 Ookayama, Meguro, Tokyo 152-8550, Japan
[10] IJCLab, CNRS/IN2P3, Université Paris-Saclay, 91405 Orsay Cedex, France
[11] RIKEN, 2-1 Hirosawa, Wako, Saitama 351-0198, Japan
[12] Department of Physics, Hokkaido University, Sapporo 060-0810, Japan
[13] Faculty of Science, Japan and Nuclear Reaction Data Centre, Hokkaido University, Sapporo 060-0810, Japan
[14] Department of Physics, Western Michigan University, Kalamazoo, MI 49008, USA
[15] Institut für Kernphysik, Technische Universität Darmstadt, 64289 Darmstadt, Germany
[16] Center for Computational Sciences, University of Tsukuba, Tsukuba 305-8577, Japan
[17] Advanced Science Research Center, Japan Atomic Energy Agency, Tokai, Ibaraki 319-1195, Japan
[18] Cyclotron and Radioisotope Center, Tohoku University, 6-3 Aoba Aramaki, Aoba, Sendai, Miyagi 980-8578, Japan
[19] Department of Physics and Astronomy, Texas A&M University, College Station 77843-4242, USA
[20] Cyclotron Institute, Texas A&M University, College Station 77843-3636, USA
[21] University of Bucharest, Atomistilor 405, 077125 Bucharest-Măgurele, Romania
[22] Dipartimento di Fisica dell'Università degli Studi di Milano, 20133 Milan, Italy
[23] INFN, Sezione di Milano, 20133 Milan, Italy
[24] Guru Jambheshwar University of Science and Technology, Hisar 125001, India
[25] Department of Physics, Kyoto University, Kitashirakawa Oiwake-Cho, Kyoto 606-8502, Japan
[26] Politehnica University of Bucharest, Bucharest, Romania
[27] GSI Helmholtzzentrum für Schwerionenforschung, Planckstrasse 1, 64291 Darmstadt, Germany
[28] Department of Physics, Okayama University, 700-8530 Okayama, Japan
[29] Department of Physics, Faculty of Science, Istanbul University, Vezneciler/Fatih, 34134 Istanbul, Turkey
[30] Department of Physics, University of Oslo, P.O. Box 1048, Blindern, 0316 Oslo, Norway
[31] Department of Chemical and Physical sciences, Walter Sisulu University, Mthatha 5100, South Africa
[32] Department of Physics, Akal University, Talwandi Sabo, Bathinda, Punjab 151302, India
[33] Physics Department, TU Munich, 85748 Garching, Germany
[34] Research Center for Electron-Photon Science, Tohoku University, 982-0826 Sendai, Japan
[35] Department of Information Engineering, National Institute of Technology, Kagawa College, Takamatsu 761-8058, Japan
[36] Shanghai Advanced Research Institute, Chinese Academy of Sciences, Shanghai 201210, China
[37] Department of Physics, Konan University, Kobe 658-8501, Japan
[38] Shanghai Institute of Applied Physics, Chinese Academy of Sciences, Shanghai 201800, China

[39] University of Chinese Academy of Science, Beijing 100049, China
[40] Department of Physics, University of York, Heslington, York YO10 5DD, UK
[41] School of Physics and State Key Laboratory of Nuclear Physics and Technology, Peking University, Beijing 100871, China

Received: 30 December 2022 / Accepted: 6 July 2023 / Published online: 11 September 2023

Communicated by Calin Alexandru Ur

Abstract Photonuclear reactions of light nuclei below a mass of $A = 60$ are planned to be studied experimentally and theoretically with the PANDORA (Photo-Absorption of Nuclei and Decay Observation for Reactions in Astrophysics) project. Two experimental methods, virtual photon excitation by proton scattering and real photo absorption by a high-brilliance γ-ray beam produced by laser Compton scattering, will be applied to measure the photoabsorption cross sections and decay branching ratio of each decay channel as a function of the photon energy. Several nuclear models, e.g. anti-symmetrized molecular dynamics, mean-field and beyond-mean-field models, a large-scale shell model, and ab initio models, will be employed to predict the photonuclear reactions. The uncertainty in the model predictions will be evaluated based on the discrepancies between the model predictions and experimental data. The data and predictions will be implemented in the general reaction calculation code, TALYS. The results will be applied to the simulation of the photo-disintegration process of ultra-high-energy cosmic rays in inter-galactic propagation.

1 Introduction

Photonuclear reaction data provide fundamental information on different aspects of nuclear structure, collective excitations, and response of nuclei to an external electric dipole ($E1$) field [1,2]. The Isovector Giant Dipole Resonance IVGDR dominates the $E1$ response of nuclei and is a widely known example of nuclear collective excitation, described as a relative dipole oscillation between the neutrons and protons. The isovector properties of the nuclear matter are constrained by systematic analyses of the $E1$ response of nuclei, such as the mean excitation energy of the (IVGDR), strength concentration around the neutron threshold, often called pygmy dipole resonance (PDR) [3,4], and static electric dipole polarizability [5–7], which corresponds to the inversely energy-weighted sum-rule value of the $E1$ strength distribution. Photonuclear reaction data and predictions are crucial for understanding various astrophysical processes, such as the r-process nucleosynthesis and intergalactic propagation of ultra-high-energy cosmic rays (UHECR). They are also crucial for applications, such as radiation shield design, non-destructive testing, γ-ray imaging, isotope production, nuclear medicine, and our understanding of biological responses to radiation.

The $E1$ response of nuclei has been widely studied in the mass region above $A \sim 90$, where nuclei exhibit bulk and smooth properties of nuclear matter with lesser dependence on the shell structure than in the lower mass region. Experimentally, the (γ, xn) reaction cross-sections, corresponding to the neutron emission channels, are often treated as a good approximation of the total photoabsorption cross-section.

The approximation is not justified in the mass region below $A = 60$ because of a comparable or even larger branching ratio to the proton decay channel than to the neutron. Furthermore, the α-decay branching ratio is not negligible in the light nuclei. Reliable prediction of the photonuclear reactions in the lower mass region is more complicated than that for heavier nuclei owing to the greater impact of effects, such as nuclear shell structure, α-clustering [15–18], isospin-selection rule, and isospin-mixing in the α-decay processes, nuclear deformation, n-p pairing, and pre-equilibrium decay processes. Additionally, the IVGDR distribution is often fragmented into several pieces, in contrast to heavier nuclei. Experimental data are scarce, particularly for charged particle decay channels and the available data are often mutually inconsistent. The parameters of the theoretical models are typically optimized for heavier nuclei. When used to predict the behavior of lighter nuclei, the predictions are insufficient in most cases. The neutron decay channel of the photonuclear reaction on ^{13}C is shown in Fig. 1 as a representative example.

The Photo-Absorption of Nuclei and Decay Observation for Reactions in Astrophysics (PANDORA) project has been initiated to study the photonuclear reaction of the light nuclei. The project relies on interdisciplinary research across the fields of experimental and theoretical nuclear physics and particle astrophysics. A precise and systematic dataset consisting of the photoabsorption cross sections and branching ratio of each decay channel will be established through the experimental nuclear physics component of the project. Two complementary methods will be employed to obtain the experimental data, i.e., virtual photon excitation through rela-

[a] e-mail: tamii@rcnp.osaka-u.ac.jp (corresponding author)

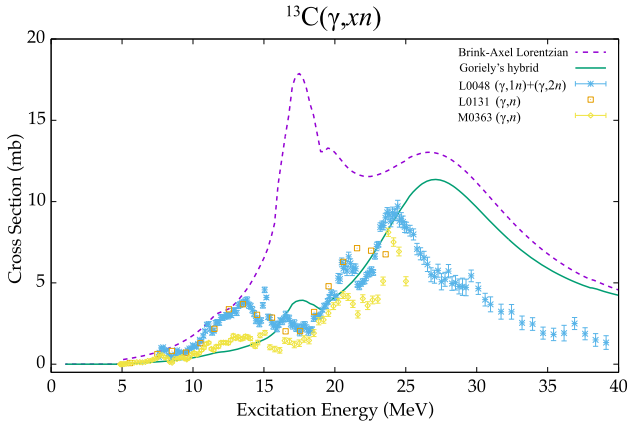

Fig. 1 Photoneutron cross sections, ^{13}C(γ, xn), as a function of excitation energy (photon-energy), showing one of typical cases where experimental data are mutually inconsistent and theoretical predictions are not satisfactory. The theoretical cross sections are calculated using the reaction code TALYS with two models, the Brink-Axel Lorentzian [8,9] (dashed line) and the Goriely's hybrid [10] (solid line). They are plotted in comparison with the available experimental data taken from the EXFOR database [11]. The data L0131 [12] (cross marks) were measured using a tagged-photon beam, M0363 [13] (diamond) with a Bremsstrahlung photon-beam, and L0048 [14] (square) through the positron-annihilation in-flight method. L0131 and M0363 (diamond) are one neutron detection data, while L0048 [14] is the integrated cross-section of the (γ, n) and $(\gamma, 2n)$ channels. The two neutron separation energy in ^{13}C is $S_{nn} = 23.7$ MeV

tivistic proton scattering at very forward angles and real photon excitation utilizing a quasi-monoenergetic γ-ray beam. The details are described in Sect. 2.1.

In the theoretical nuclear physics portion of the project, models will be developed to predict the photoabsorption cross-sections and decay branching ratios. The employed models include Antisymmetrized Molecular Dynamics (AMD) [19,20], Random Phase Approximation (RPA) based on the energy density functional (EDF) [24], beyond-mean-field Relativistic Nuclear Field Theory (RNFT) [21–23] and Quasiparticle Phonon Model (QPM) based on EDF [25,26], a large-scale shell model [27], and ab initio approaches. Predictions will be evaluated using the experimental data to estimate model uncertainties and for further development.

The obtained experimental data and model predictions will be implemented in a general reaction calculation code, TALYS to be made available for applications in various fields. An important outcome of the PANDORA project will be a better characterization of the photo-interactions of UHECR, which is an essential ingredient of the theoretical modeling of their extra-galactic propagation and acceleration in astrophysical sources. This phenomenon is briefly described in Sect. 5.

The remainder of this paper is organized as follows. The experimental methods for measuring the photoabsorption cross-sections and decay branching ratios are described in Sect. 2. The theoretical models are described in Sect. 3. The background of UHECR physics and application of the photonuclear reaction information to the extra-galactic propagation of UHECRs are introduced in Sect. 5. Other potential applications are briefly discussed in Sect. 6 followed by a summary and outlook in Sect. 7.

2 Experimental nuclear physics

An overview of the experimental methods is provided in Sect. 2.1. Then, the three main experimental facilities, RCNP, iThemba LABS, and ELI-NP of the PANDORA project, are introduced followed by other related facilities.

2.1 Methods

The experimental nuclear physics part of the PANDORA project aims to systematically measure the photoabsorption cross-sections and the p, n, α, and γ decay branching ratios for stable nuclei in the mass region below $A = 60$. Two modern experimental methods will be employed. One is the virtual photon excitation through relativistic proton scattering applicable at the Research Center for Nuclear Physics (RCNP) in the Osaka University, Japan, and iThemba LABS, South Africa [5,28,29]. The other method is real photon excitation through high-intensity quasi-monoenergetic γ beams produced by the laser Compton scattering (LCS) at Extreme Light Infrastructure-Nuclear Physics (ELI-NP), Romania. The combination of complementary facilities is essential for obtaining a high-quality systematic dataset. The ELI-NP facility [30] is under construction as a next-generation high-brilliance high-resolution LCS facility following the successful operation of the LCS facilities in Japan [31,32] and in the US [33].

To establish consistency among the data measured at the three facilities, ^{27}Al was chosen as the reference nucleus for each experimental campaign owing to its ease of fabrication and treatment, natural mono-isotopic abundance, availability of the (γ, abs) data [34], and prediction of reasonably large branching ratios for each of the p, n and α decay channels with relatively low threshold energies. All of these three facilities can identify the nuclear excitation energy with a high resolution of 100 keV or higher. This excellent energy resolution is beneficial for establishing mutual data consistency among the three facilities for discrete states, broad resonances, and related fine structures.

Almost all the stable nuclei below the mass of $A = 60$ are involved in the photodisintegration path of the UHECR nuclei in the intergalactic propagation (see Sect. 5). Because it is impractical to measure the photonuclear reactions for all the stable nuclei involved, a limited set of nuclei will be measured to allow the benchmarking of the nuclear model

predictions. The selection of the candidate nuclei is listed below.

- reference target: ^{27}Al.
- first cases and importance of α-decay: ^{12}C and ^{16}O.
- light nuclei: ^{6}Li, ^{7}Li, ^{9}Be, and ^{10,11}B.
- $N = Z$ nuclei, α-cluster effect and deformation: ^{24}Mg, ^{28}Si, ^{32}S and ^{40}Ca.
- isospin selection-rule in α-decay: isotope pairs of ^{10,11}B, ^{12,13}C, ^{16,18}O and ^{24,26}Mg.
- $N > Z$ nuclei and multi-neutron emission: ^{13}C, ^{18}O, ^{26}Mg, ^{48}Ca and ^{56}Fe.
- A-odd and odd-odd nuclei: ^{7}Li, ^{9}Be, ^{10,11}B, ^{13}C, ^{14}N.

Self-supporting pure targets or chemical compounds with high isotopic enrichment or high natural isotopic abundance will be used. We note that (γ, α) measurements on ^{9}Be, ^{12}C and ^{16}O at the HIγS facility are reported [35–37] although the excitation energies are well below the IVGDR.

2.2 Virtual photon excitation at RCNP

The excitation energy distribution of the $E1$ reduced transition strength, $dB(E1)/dE_x$, will be measured using the virtual-photon excitation method at the RCNP, Osaka University, where two cyclotrons will be used in a cascade to accelerate a proton beam to 392 MeV. The Grand Raiden spectrometer [38] is placed in the zero-degree inelastic scattering mode [28,39] to measure the scattered protons at 0°–3° degrees (left panel in Fig. 2), and at 4.5° and 6.5° covering the scattering angular range of 3.5°–7.5° in the Grand RAiden Forward (GRAF) mode [40] (right panel in Fig. 2). The beam is transported to the zero-degree beam dump (wall beam dump) in the zero-degree (GRAF) mode. The beam dumps are well separated from the target position and shielded by concrete to reduce the radiation entering the decay detectors. A proton beam at 392 MeV is employed to cover the excitation-energy range of 7–32 MeV in the zero-degree mode. The details of the experimental technique can be found in Ref. [28].

Multipole decomposition analysis of the (p, p') reaction is well established at the RCNP [5,6]. The angular distribution of the (p, p') cross-sections will be fitted by the sum of theoretical angular distributions for several multipoles to extract the $E1$ component, which dominates at 0°. The $E1$ cross-section at 0° is converted to the $E1$ reduced transition strength $B(E1)$ by using the Coulomb excitation calculation with the Eikonal approach.

A silicon detector array, SAKRA (Si Array developed by Kyoto and osaka for Research into Alpha cluster states) [41], will be placed around the target position for coincidence measurement of decay charged particles (Fig. 3). SAKRA consists of double-sided silicon strip detectors (DSSSDs) with a

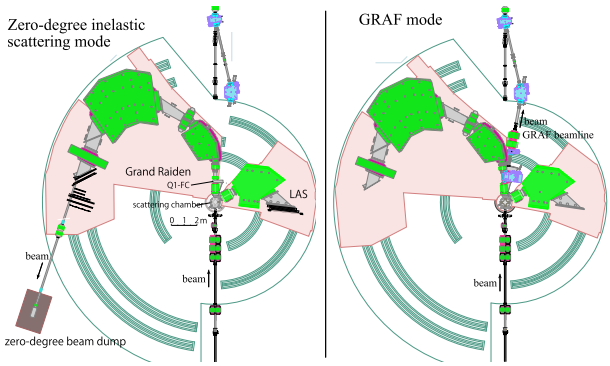

Fig. 2 Left panel: Grand Raiden spectrometer in the zero-degree inelastic scattering mode [5]. The beam is transported in the spectrometer and is stopped in the zero-degree beam dump. Right panel: GRAF mode [40] for the measurement with placing the spectrometer at an angle larger than 4.5 degrees. The beam is transport in the GRAF beam line and is stopped at a beam dump (not shown in the figure) located 20 m downstream from the scattering chamber

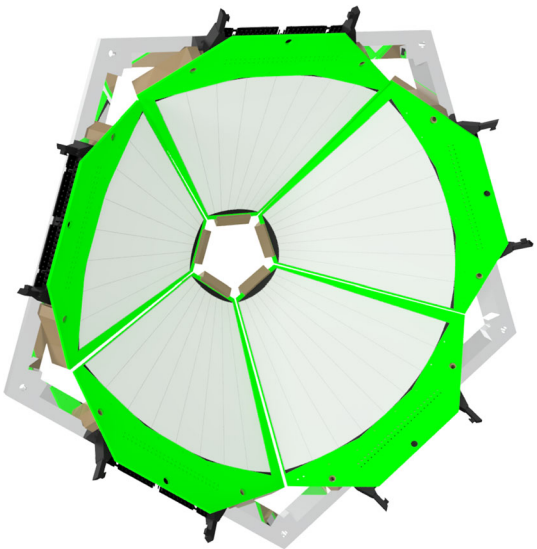

Fig. 3 Illustration of the silicon detector array SAKRA developed at Osaka University for charged-particle decay detection in five DSSSD configuration with a thickness of 500 μm

thickness of 500 μm with the detector model name of MMM from Micron Semiconductor Limited. SAKRA covers a solid angle of approximately ∼ 25% of 4π at backward angles with respect to the beam direction. The lowest detectable energy is ∼ 0.5 MeV. The maximum detectable energy without penetration of the detector is 8.2, 11.0, and 33.0 MeV for p, d, and α particles, respectively.

Eight large-volume $LaBr_3$ detectors (3.5"φ–8" L) [42,43] will be placed around the target chamber for decay γ-ray detection [40], as shown in Fig. 4 . The distance from the target position to the front surface of the $LaBr_3$ detectors is approximately 200 mm. A beam-time proposal for the first PANDORA experiment at the RCNP was approved and is

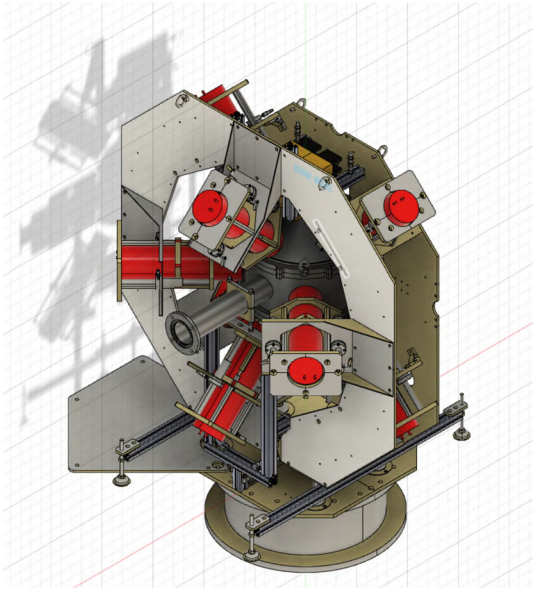

Fig. 4 Eight large-volume $LaBr_3$ detectors placed around the target chamber accommodating the SAKRA (view from the upstream side of the beam)

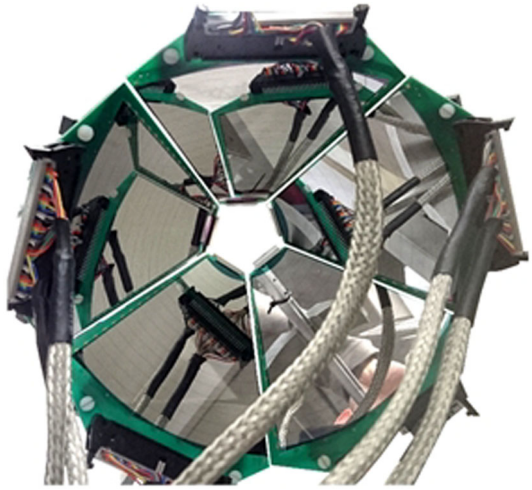

Fig. 5 Silicon-strip detector array, CAKE, at iThemba LABS in the standard single-layer configuration

scheduled in year 2023. The planned targets are ^{12,13}C, ^{27}Al, and ^{24,26}Mg for the decay measurement in coincidence with the scattered protons and ^{10,11}B only for the scattered protons.

2.3 Virtual photon excitation at iThemba LABS

The dispersion-matched 200-MeV proton beam produced by the Separated Sector Cyclotron (SSC) at iThemba LABS will be used to measure the photoabsorption response of the target nuclei. The scattered protons will be momentum-analyzed with a $K = 600$ magnetic spectrometer [29]. The spectrometer consists of five active elements, i.e., a quadrupole, two dipoles, and two trim coils (K and H). The focal plane detector consists of two multi-wire drift chambers (MWDC)s that measure the horizontal and vertical positions of the scattered particles, and two plastic scintillating detectors that provide information on the energy deposited at the focal plane. The excitation energy is determined from the horizontal position of the first MWDC. Particle identification and halo rejection are accomplished using the energy deposited in the scintillators and the time between the trigger event and the following reference radio-frequency signal from the accelerator system.

For this study, the K600 spectrometer will be operated in the zero-degree and small-angle configurations, in which the center of the spectrometer will be at 0° and 4°, respectively, resulting in data acquired over a total angular range of 0°–6°. This allows for extraction of the photoabsorption cross-section from the (p, p') data by applying multipole decomposition analysis (MDA) of the measured data [5]. The MDA is based on model predictions of the angular distribution shapes of the different multipolarities contributing to the spectra. For each discrete transition or excitation energy bin, the experimental angular distribution is fitted by employing the least-squares method to the sum of calculated angular distributions, weighted with coefficients corresponding to the different multipolarities of the transitions. Owing to the increasing complexity of contributions from different multipoles at higher momentum transfers, MDA is more reliable and effective in the angular range below 10°. By combining the 0° and 4° configurations, five to seven data points can be extracted in the 0°–6° angular range.

Coupled with the K600 spectrometer, Coincidence Array for K600 Experiment (CAKE) [44] will be used to measure the subsequent particle decay from the excitation of the giant dipole-resonance (GDR). In the standard configuration, CAKE comprises five DSSSDs of the MMM design from Micron Semiconductor Limited, arranged in a lamp-shaped configuration as shown in Fig. 5. The detectors are 400-μm thick with 16 ring channels on the junction side of the detector and eight sector channels on the ohmic side. The limitation in proton energy detection (7 MeV) due to the thickness of the detectors can be overcome by arranging the detectors in a double-layer configuration. The array will be arranged in the first experiment to cover the maximum solid angle (25%) with a single-layer configuration. One section of the array will be set up as the double layer. This allows the testing of the double-layer configuration for future PANDORA experiments. Particle identification will be carried out using the time-of-flight technique, as shown in Ref. [44], and energy excitation energy vs silicon energy matrices can be constructed for different decay channels. The array will be coupled to the spectrometer in both angular configura-

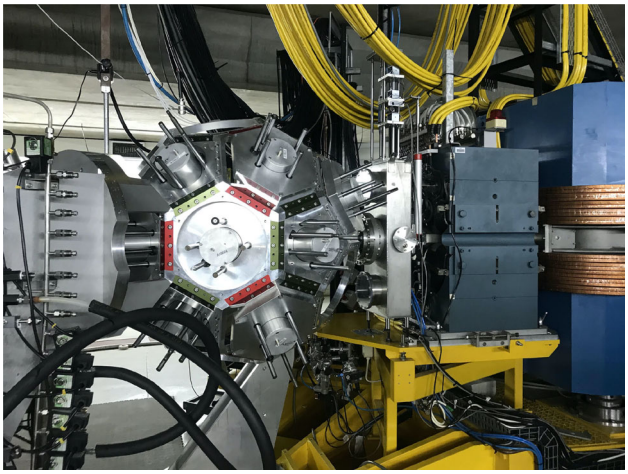

Fig. 6 African LaBr Array (ALBA) coupled with the K600 magnetic spectrometer at iThemba LABS

tions. The measurement of all the decay channels is crucial for simulating the evolution of energy and composition in the propagation of UHECRs. Therefore, the de-excitation of GDR through γ-ray emission will also be measured by placing large-volume $LaBr_3$:Ce detectors from the African LaBr Array – African Lanthanum Bromide Array (ALBA) – around the scattering chamber, as shown in Fig. 6. The ALBA comprises up to 21 large-volume $LaBr_3$:Ce detectors (3.5"ϕ–8"L), which can be arranged at an average distance of 18–20 cm from the target. These detectors will be utilized only in the K600 zero-degree configuration because of the limitation imposed by the background originating from the beam dump in the finite-angle setting. The γ-decay information will also be used to extract the branching ratio of particle decays into excited states by detecting the γ-rays from the daughter states.

2.4 Real photon excitation at ELI-NP

The focus of the ELI-NP facility [30,45,46] is to directly measure the decay strength in different channels following a population of high-energy states using real photons from a γ-ray beam. The ELI-NP facility has two main approaches to photonuclear physics. One of these systems is a 10 PW high-power laser beam line [47]. However, for this study, the main beam-line of interest is the high-brilliance, low-bandwidth γ-ray beam produced by Compton backscattering of a regular laser off an electron beam. This system, called variable energy gamma (VEGA), will consist of an electron storage ring coupled to a Fabry–Pérot optical cavity. The energy of the circulating electrons can be steplessly varied in the range of 234–742 MeV and photons from two different laser configurations, covering two different energy ranges, one at $\sim$ 1 μm and the other at $\sim$ 0.5 μm, respectively, will be able to cover γ-ray energies in the range of 1–19.5 MeV.

Table 1 Main predicted parameters of the VEGA system at ELI-NP.

Parameter	Limit
Energy	$\leq$ 19.5 MeV
Polarisation	$\geq$ 95%
Bandwidth (FWHM)	$\leq$ 0.5%
Peak spectral density	$\geq 5000\ s^{-1}eV^{-1}$
Off-Peak background density	$\leq 1.0 \times 10^{-2}\ s^{-1}eV^{-1}$
Divergence (FWHM)	$\leq 1.5 \times 10^{-4}$ rad
Repetition rate	$\lesssim$ 72 MHz
Beam intensity at 10 MeV	$\sim 2.5 \times 10^{8}\ s^{-1}$

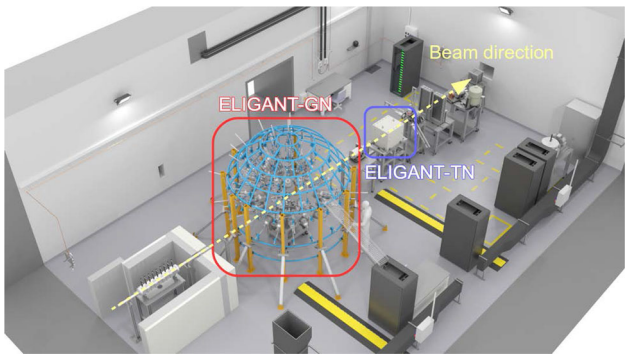

Fig. 7 ELI-NP experimental setup for experiments above the neutron threshold

Owing to the nature of the Compton backscattering process, the beam is expected to be almost completely polarized. The bandwidth of the beam is predicted to be less than 0.5%, making it an ideal probe for the type of resonant structures expected in the light nuclei studied in the PANDORA project. The primary parameters of the VEGA system are listed in Table 1.

Several experimental setups are currently being prepared for photonuclear measurements at ELI-NP related to nuclear structure and photonuclear reactions. The reaction studies, with the most significant relevance to the project discussed here, consist of both charged particle and neutron detection following nuclear excitation with the γ-ray beam. For neutron detection, two different setups were constructed at the ELI-NP facilities, i.e., the ELIGANT Thermal Neutron (ELIGANT-TN) setup [48] for high-precision cross-section measurements for (γ, xn) reactions, and ELIGANT Gamma Neutron (ELIGANT-GN) [48–50] to investigate the correlations and competition between the neutron and γ-ray decay channels from the states above the neutron threshold. The experimental area is shown in Fig. 7.

ELIGANT-GN consists of 34 large-volume $LaBr_3$:Ce and $CeBr_3$ detectors of length 76 mm and diameter 76 mm for high-energy γ rays. For neutron detection, 36 liquid scintillator EJ-301 type detectors will be used at a distance of 1.5 m

from the target for high-energy neutrons, and 25 lithium-glass GS20 type detectors will be used at a distance of 1 m from the target for low-energy neutrons. The large-volume crystal scintillators have a two-fold role. One is to identify weak one- and two-step branches from the GDR states and the other is to provide a clear time reference for neutron energy measurements via time-of-flight in liquid and glass scintillators. In a recent paper on the commissioning [50], the total γ-ray detection efficiency was estimated to be 1% at an energy of 10 MeV. The liquid scintillators have an estimated efficiency of 1% at a neutron energy of 10 MeV and up to 2.5% at a neutron energy of 2 MeV. Below 1 MeV, the efficiency decreases rapidly. However, the inclusion of the lithium-glass scintillators can provide low-energy neutron detection with an efficiency of 0.5% at a neutron energy of 250 keV.

The ELIGANT-TN consists of 28 tubes filled with ^{3}He and embedded in a polyethylene matrix. The efficiency of the neutron counter is 38% over the complete, predicted neutron energy range. This feature is essential because it means that the energy spectrum of the emitted neutrons does not bias the measured cross-section. Although the detector is used with neutrons moderated to thermal energies, the average neutron energy can still be obtained using the ring-ratio method [51], providing additional information for comparison with different theoretical approaches. Owing to the flat efficiency, higher-order neutron emission cross-sections can be disentangled from the total neutron emission cross-section using the direct multiplicity sorting procedure, which is well described in the references [52–54].

A common assumption in the measurements of the GDR cross-section for heavy nuclei is that the total decay of the GDR is very close to that of the neutron decay channel. However, this not necessarily the case for nuclei to be studied in the PANDORA project. Besides internal transition decay via γ-rays, a significant part of the decay could occur via charged particles, such as protons and α particles. At ELI-NP, charged particle reaction studies will primarily be carried out with the silicon-strip detector array, ELI Silicon Strip Array (ELISSA), and large time-projection chamber ELI-TPC [55]. For experiments within the PANDORA project, the ELI-TPC can be operated in the stand-alone mode for rare reaction channels with gas targets. ELISSA, in the configuration proposed in the technical design report, consists of three rings of twelve $X3$ position-sensitive detectors [56] in a barrel-like configuration and two end cap assemblies. To integrate ELISSA with ELIGANT-GN, a new, compact configuration is required. However, this allows us to investigate multiple-particle reactions, for example, (γ, np) or $(\gamma, \mathrm{n}\alpha)$ in the cases of α-cluster nuclei with excess neutrons such as ^{13}C.

For this study, the γ-ray beam provided by ELI-NP will be used with 50–100 keV energy resolution in the energy range from the particle separation thresholds up to the maximum available γ-beam energy. The proposed targets are neither very rare nor radioactive. Thus, they are not limited by the beam size at the experimental point and can accept beam spots of a few millimeters. For the same reason, the beam intensity is not a sensitive issue in this study, and a lower intensity is acceptable by introducing a time structure in the beam. This sacrifice in intensity can easily be countered using thicker targets. It would have the additional benefit of increased accuracy and precision in the neutron energy measurements, as well as adding the possibility of separating $(\gamma, 1\mathrm{n})$ and $(\gamma, 2\mathrm{n})$ cross-sections in the ELIGANT-TN for events above the two-neutron separation threshold. The use of fully polarized beams allows the separation of the $E1$ and $M1$ responses, as well as the separation of s-wave and p-wave neutron emissions. For a given isotope, different target thicknesses can be produced for different energies, keeping the total reaction rate as constant as possible in the detector setup. This ensures that the statistical uncertainties remain similar and that systematic uncertainties related to the count rate in the detector system are minimized.

2.5 Other related facilities

2.5.1 HIγS

The High Intensity γ-ray Source (HIγS) [57] is a joint project between the Triangle Universities Nuclear Laboratory (TUNL) and the Duke Free Electron Laser Laboratory (DFELL). The HIγS facility is shown schematically in Fig. 8. An electron beam is generated in a photo-cathode microwave electron gun, bunched, and pre-accelerated to energies of $E_{e^-} = 0.18$–0.28 GeV in an electron linear accelerator. The subsequent booster synchrotron can ramp the energy up to 1.2 GeV before the electron bunches are injected into the Duke electron storage ring. Within the storage ring, the free electron laser (FEL) is powered by an electron beam.

The ring electrons are deflected by several wiggler magnets placed in the storage ring and they emit horizontally or circularly polarized FEL photons with variable wavelengths in the range 190–1060 nm. These photons are reflected by FEL mirrors and collide with another electron bunch at the collision point. In the laser Compton backscattering (LCB) process, the photon energy can be boosted up to 100 MeV with a total flux on the target in the order of $\sim 10^8\ \gamma/s$ depending on the scattering angle. The LCB beam energy can be tuned by adjusting the electron and FEL energies, respectively. Owing to the polarization conservation of the Compton backscattering process, a linearly or circularly polarized high-energy LCB photon beam is produced. The high-intensity photon beam passes the FEL mirror and is collimated approximately 60 m downstream of the collision point. Depending on the spatial distribution of the backscattered

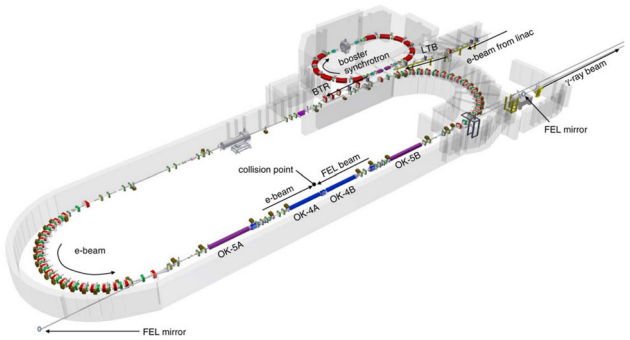

Fig. 8 Scheme of the HIγS facility. For details, see Ref. [57]. Reprinted with permission from [57]

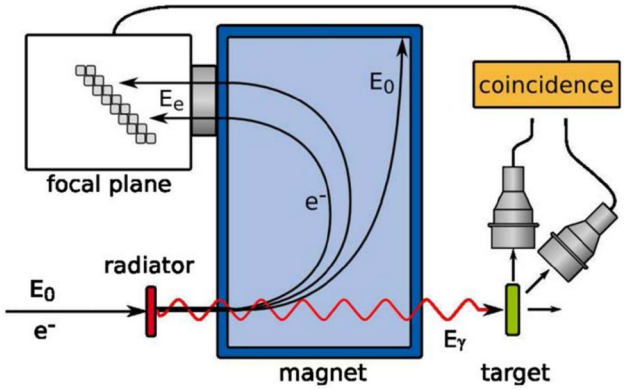

Fig. 9 Principle of photon tagging. For details, see Ref. [80]. Reprinted figure with permission from [80]

photons and collimator size, the typical full width at half maximum (FWHM) of the beam energy profile is 1–3% of the peak energy.

Two experimental halls with dedicated detector setups [58] are located in the upstream target room (UTR) and the Gamma Vault, which use a high-energy photon beam to perform nuclear physics experiments. Several NRF studies have been performed in the past decades to determine the spin and parity quantum numbers of excited states [59–62], investigate collective excitation modes in deformed nuclei [63–66], and extract photoabsorption cross-sections [67–70] and photon strength functions [71,72]. Furthermore, (γ, n) reactions in the light nuclei [73–75] and in the Fe-Ni region were measured [76,77]. Very recently, the γ-decay of the IVGDR into the ground-state rotational band in the deformed nucleus ^{154}Sm was observed [78], demonstrating the the potential of LCB beams for the investigation of photoabsorption cross-sections and decay channels for physics goals in PANDORA. For a recent review article on nuclear structure studies and applications with a photonuclear reaction below and above particle emission thresholds see Ref. [79].

2.5.2 NEPTUN at S-DALINAC

The photon-tagger NEPTUN [80] operating at the S-DALINAC [81] of the Institute for Nuclear Physics of TU Darmstadt provides a beam of energy-tagged and, therefore, quasi-monoenergetic photons. The basic principle is illustrated in Fig. 9.

The electron beam of S-DALINAC with energy E_0 impinges on a thin radiator target, producing bremsstrahlung photons. The reacted electrons are momentum-analyzed via dispersion in a large dipole magnet and detected using a focal plane consisting of scintillator strips coupled to a silicon photomultiplier. The energy of the generated photon ($E_\gamma = E_0 - E_e$) is determined from the remaining energy of the reacted electron E_e and E_0, neglecting the recoil energy transferred to the atom in the radiator in the bremsstrahlung process. The coincident measurement of the induced photonuclear reactions on the samples in the experimental setup, and the reacted electron enables to 'tag' the initial photon energy and thus, conduct experiments with quasi-monoenergetic photon beams. Tagged photons in the energy range of 5–35 MeV can be produced with maximum spectral photon densities of 103 photons/keV/s after collimation with a solid angle of 3 mrad. The experimental setups are located 5 m downstream of the photon tagger, NEPTUN. Currently, two possible setups exist: the GALATEA LaBr-detector array to detect high-energy photons, and the fast target changer PROTEUS. The latter is combined with a large-volume CeBr scintillator positioned in-beam downstream of PROTEUS to measure photoabsorption cross sections via total photoabsorption directly. The advantage is that the complete absorption is measured directly and independently of any particular exit channel. Thus, future experiments at NEPTUN and PROTEUS have the potential to provide complementary datasets for the photoabsorption cross sections in the mass region studied in PANDORA.

2.5.3 SLEGS at SSRF

The Shanghai Laser Electron Gamma Source (SLEGS) depicted in Fig. 10 is the γ-ray production beam line built at the Shanghai Synchrotron Radiation Facility (SSRF). The slant-scattering mode was employed for the first time to systematically produce energy-tunable γ-ray beams by LCS of 10.64 μm photons from a CO_2 laser with 3.5 GeV electrons in the storage ring. The SLEGS officially completed its commissioning run between July and December 2021 [82]. An interaction chamber dedicated to the slant scattering was constructed [83]. The energy range of the LCS γ-rays produced at SLEGS is 0.66–21.7 MeV. The maximum energy of the γ-ray beam is 0.66 MeV at the slant-scattering angle 20° and 21.1 MeV at 160°, while the highest achievable energy is 21.7 MeV in the back-scattering at

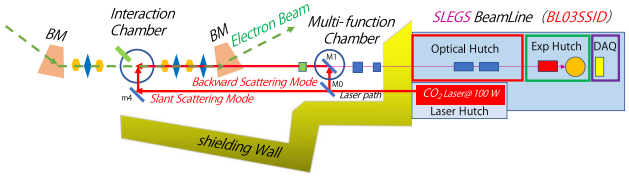

Fig. 10 Gamma-ray production beam-line, SLEGS, built at the Shanghai Synchrotron Radiation Facility (SSRF)

180°. The CO_2 laser is vertically introduced into the interaction chamber, transported through a set of mirrors and convex lenses, and focused at the collision point with 3.5 GeV electrons. The laser optical elements are mounted on a turn table inside the interaction chamber to continuously change the slant-scattering angle from 160° to 20°. The γ-ray flux at the production point is 2.1×10^4 at 20°, 2.5×10^6 at 90°, and 1.2×10^7 at 180° for the 5 W (maximum 100 W) CO_2 laser and 300 A electron beams. The γ-rays are directed to the experimental hutch through the double collimator system [84]. The energy resolution of γ-ray beams at the target position is 2–15% in the full width at half maximum, depending on the slant-scattering angle, provided that the γ-ray emission angle is confined to be less than 0.45 mr with the collimator system. The four types of detectors meet the versatility requirements of nuclear physics experiments. This makes it possible to perform nuclear resonance fluorescence, flat-efficiency neutron, high-resolution neutron time-of-flight, and low-energy charged-particle measurements for photonuclear reactions [82]. In the PANDORA project, from the iron group (Fe-Co-Ni) to the lithium nuclei, one can investigate the neutron decay of the giant- and pygmy-dipole resonances, mainly $(\gamma, 1n)$ cross-sections, decay branching ratios to excited states in the residual nuclei, and the charged-particle decay, mainly (γ, p) and (γ, α) cross-sections.

2.5.4 *SCRIT electron scattering facility for short-lived exotic nuclei*

A ground-breaking electron-scattering facility has been built at RIKEN, Japan, and is currently in operation. The Self-Confining RI Ion Target (SCRIT) electron scattering facility is dedicated to short-lived exotic nuclei far from the stability as shown in Fig. 11.

Structural studies of exotic nuclei through electron scattering are possible at the SCRIT facility because of the novel target-forming technique combined with a high-energy electron beam [85]. The SCRIT technique provides high luminosity, $\sim 10^{27}\,\mathrm{cm}^{-2}\,\mathrm{s}^{-1}$, enough for elastic scattering with a very small number of target ions, typically of the order of $10^9\,\mathrm{cm}^{-2}$ [86].

In addition to the ground-state charge density profile of short-lived exotic nuclei through elastic electron scattering,

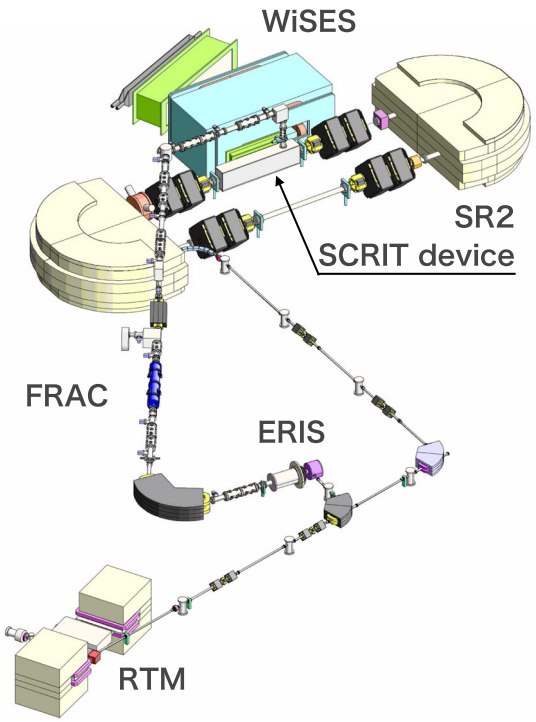

Fig. 11 SCRIT electron scattering facility at the RIKEN RI Beam Factory

their $E1$ responses will also be accessible at the SCRIT facility. The $E1$ responses of exotic nuclei have been studied only through Coulomb excitation reactions in nucleus-nucleus collisions. Because it is not a purely electromagnetic reaction, its interpretation has been questioned.

The inelastic electron-scattering cross section at an ultra-forward angle $\theta \sim 0°$ is known to be related to the photonuclear cross-section through virtual-photon theory. Detecting the inelastic electron scattering off exotic nuclei at a very forward angle allows the determination of the total photoabsorption cross-section. It should be stressed that at this facility, the full GDR region can be covered with an electron beam energy of $\sim$ 100 MeV [87], which was previously limited to a few cases even using energetic RI beams.

3 Theoretical nuclear physics

In the nucleus rest frame, at typical UHECR energies of 10^{19}–10^{21} eV, the cosmological microwave background (CMB) photons are boosted to energies in the range of a few hundreds of keV up to a few hundreds of MeV. The interaction process between the UHECRs and the CMB is dominated by the GDR at photon energies below 30–50 MeV, and to a lesser extent, by the quasideuteron emission for intermediate energies (between 50 and 150 MeV) and the pion photoproduction at energies above 150 MeV [88]. Nuclei are pho-

todisintegrated by emitting nucleons through (γ, n), (γ, p), $(\gamma, 2n)$, and other reactions. During the photodisintegration path from Iron to protons, it is necessary to describe the dipole strength of the involved nuclei accurately. It should be noted that a large number of nuclei along this path are unstable.

The photoreaction cross-sections can be estimated using the TALYS nuclear reaction code [89], which considers all types of direct, pre-equilibrium, and compound mechanisms to estimate the total reaction probability and the competition between the various open channels. Therefore, the photoreaction cross-section is usually estimated at energies of up to 50 MeV. Using a large variety of nuclear structure models to describe such cross-sections is relevant because it allows us to estimate the corresponding typical theoretical error.

3.1 RPA-EDF

An RPA with an effective EDF is a standard tool for calculating the $B(E1)$ distributions of nuclei. The RPA-EDF describes $E1$ and other modes, such as monopoles or quadrupoles, in nuclei covering the entire nuclear chart for each effective EDF. They provide systematic reproduction of the experimental data, including the collective properties of the giant resonances. They also predict the PDR, also called the low-lying electric dipole (LED) mode, in a broad mass region.

The RPA equation with EDF is derived as a small-amplitude vibration or linear response to external perturbations of time-dependent density functional theory (DFT) [90]. Based on the DFT that contains only one-body densities, the RPA-EDF equation is formulated from the one-body densities calculated from the single-particle wave functions of an A-nucleon system. Compared to other calculations, this approach dramatically reduces the computational cost and is applicable to heavy nuclei and infinite nuclear matter. Its predictability is less reliable for very light nuclei (typically $A < 10$) than for heavy nuclei.

In the RPA-EDF, collective vibrational modes are described as a superposition of single particle-hole excitations, providing a straightforward interpretation of the properties of these modes. However, owing to a lack of many-particle-many-hole excitations, the RPA-EDF cannot describe the spreading width, failing to reproduce experimental widths of giant resonances. A spreading width of 1–2 MeV is often assumed to reproduce the experimental widths.

The RPA-EDF is powerful for describing the photonuclear cross-section to be measured in the PANDORA project. Developments to improve the predictions of light nuclei are currently in progress. A Monte Carlo calculation has recently shown that a few Skyrme-EDF parameters are correlated with the peak energy of the GDR [91]. This enables the optimization of the Skyrme-EDF parameters to reproduce the peak energy of the measured GDR. We plan to develop a new set of Skyrme-EDF parameters, which better describe the $E1$ strength distribution than that currently available.

3.2 Relativistic nuclear field theory (RNFT)

The RNFT was developed over the last couple of decades as a response to novel challenges in nuclear structure and astrophysics. The RNFT emerged as a synthesis of late extensions of the Landau–Migdal Fermi liquid theory, Copenhagen–Milano nuclear field theory (NFT), and quantum hadrodynamics (QHD) [92–98]. The QHD, being a covariant theory of interacting nucleons and mesons, constrained by low-energy quantum chromodynamic (QCD), turned out to be successful at the mean-field level [99–103]. The idea of fine-tuning meson masses and coupling constants and introducing a nonlinear scalar meson led to an excellent quantitative description of the nuclear ground states. Thus, the QHD provides a connection between the low-energy QCD scale and nucleonic scale of complex strongly-interacting media. The time-dependent version of the relativistic mean field (RMF) model and the response theory built on it have allowed for a good description of the positions of collective vibrational states in the relativistic random phase approximation (RRPA) [104–106], or, for the superfluid systems, by the relativistic quasiparticle random phase approximation (RQRPA) [107,108]. The RMF and R(Q)RPA form the content of the covariant density functional theory (CDFT), which performs very well and provides a better description of nuclear properties than non-relativistic DFTs.

First, the many-body correlations associated with temporal non-localities of nucleonic self-energy and effective interaction were considered in the extensions of the CDFT. Namely, the first step connecting single-nucleon and vibrational degrees of freedom was made by RNFT [92–96,109], a relativistic version of the original NFT [110–116], and the extended theory of finite Fermi systems [117,118], which accounts for the in-medium retardation effects of the meson exchange, missing in CDFT, in the leading approximation. The latter is based on the emergence of collective degrees of freedom, such as vibrations (phonons) caused by coherent nucleonic oscillations. An order parameter associated with qPVC vertices provides consistent power counting and controlled truncation schemes. In the implementations with effective interactions, the quasiparticle – vibration coupling (qPVC) vertices and frequencies, which provide the most important contributions to the nucleonic self-energy and effective interaction beyond the CDFT, can be well approximated by the R(Q)RPA. The nonperturbative treatment of the qPVC effects is based on the time ordering of two-loop and higher-order diagrams, containing multiple exchanges of vibrations between nucleons, and evaluating their contributions to one- and two-nucleon propagators. The leading approximation to the nucleonic self-energy includes 'one

(quasi) particle coupled to one phonon' $1q\otimes phonon$ configurations [92,119], while 'two (quasi) particles coupled to one phonon' $2q\otimes phonon$ or $2phonon$ configurations enter the extended induced interaction [94,95]. Later generalizations of the RNFT were devoted to configurations of higher complexity ($np-nh$, or $2q\otimes Nphonon$) [96], inclusion of isospin-flip phonons [109,120], ground state correlations caused by qPVC [98], and finite-temperature effects [121,122].

The nuclear response theory with the qPVC effects, which was developed within this formalism in a parameter-free way and called relativistic quasiparticle time blocking approximation (RQTBA), provides a high-quality description of the gross properties of the giant resonances [94,123,124] and some fine features of excitation spectra at low energies [97,125] in both neutral and charge-exchange channels for medium-mass and heavy nuclei. In particular, the isospin splitting of the pygmy dipole resonance has been explained quantitatively [125], and the beta-decay half-lives were reproduced successfully in the first version of the proton-neutron RQTBA [97]. The generalized RQTBA with multiphonon couplings [96] unifies the theory of high-frequency collective oscillations and low-energy spectroscopy [126]. The essential features of the RNFT are: (i) it is constrained by the fundamental underlying theories, such as QCD, and hence, consistent with the Lorentz invariance, parity invariance, electromagnetic gauge invariance, isospin and chiral symmetry (spontaneously broken) of QCD; (ii) it includes the effects of nuclear superfluidity on equal footing with the meson exchange and qPVC, so that it applies to open-shell nuclei; and (iii) it is a parameter-free extension of the CDFT, which is applicable and demonstrates high performance almost throughout the entire nuclear chart, from the oxygen mass region to super-heavy nuclei [119,127].

Recently, the R(Q)TBA was re-derived in a model-independent equation of motion (EOM) framework based on the bare fermionic Hamiltonian without applying time-blocking operators [126]. The EOM formalism allows for ab initio descriptions and further extensions of RNFT. Overall, the original and extended versions of the R(Q)TBA demonstrate significant improvements in describing nuclear collective excitations and soft modes compared with the standard (Q)RPA theories.

3.3 EDF-QPM

A microscopic approach based on self-consistent EDF and quasiparticle random phase approximation (QRPA) formalism complemented by multiphonon configurations was developed and used in various studies on the nuclear structure of low-energy excited states, pygmy, and giant resonances [25,128]. Currently, the EDF + three-phonon QPM theory [26,129] is a successful method that allows for a unified description of low-energy single-particle and multiphonon states and giant resonances. For example, a uniform treatment is required to separate the multiphonon states, PDR and GDR strengths. An essential advantage of the QPM compared to other methods with quasiparticle-phonon coupling is the use of sufficiently large configuration spaces, including up to three-particle-three-hole ($3p-3h$) components. They are the most important prerequisites for quantitative descriptions of the fine and coarse properties of nuclear spectral functions and the description of nuclear data with highest accuracy [25,26,128,130–132]. Furthermore, the approach was able to predict the nuclear structural properties and dynamics of new modes of nuclear excitation at low energies, and in particular, the PDR and its higher multipole extension, and the pygmy quadrupole resonance (PQR) [133]. In this respect, the calculations of the branching ratios to the ground and low-energy excited states serve as highly sensitive observables for distinguishing simple one-particle-one-hole ($1p-1h$)-type configurations and multiphonon structures [132,134].

With this study, we intend to apply the EDF–QPM approach to studies of electric and magnetic low-energy excitations with complex structures, pygmy, and giant resonances in atomic nuclei with masses around and below $A = 60$. Calculations of the transition strengths and branching ratios of PDR and GDR to the lowest-lying excited states and ground state can provide insight into the mechanism of decay of these excitation modes [132]. The PDR can contribute to the neutron capture cross-sections of the nuclear reactions of the s- and r-processes of nucleosynthesis in astrophysics [130,135,136]. In addition, multiparticle-multihole excitations related to nuclear polarization can cause redistribution and fragmentation of the low-energy $1p-1h$ strength, which can significantly affect the radiation capture cross-sections [26,136]. In this regard, EDF–QPM spectral distributions can be implemented in nuclear reaction code to evaluate and predict the nuclear reaction rates of astrophysical importance.

3.4 AMD

The electric dipole states of light nuclei will be studied using the AMD model [19,20] combined with the shifted-basis method [137] or the real-time evolution method (REM) [138]. Furthermore, the decay branches (n, p, γ, and α decays) will also be studied within the same framework using the Laplace expansion method [139].

The AMD framework uses the Slater determinant wave function of the nucleon wave packets to describe the structure and response of the atomic nuclei. To incorporate with the particle-hole states, which are relevant to the electric dipole states, the shifted-basis method or recently developed REM will be combined with AMD. The shifted-basis method has already been applied to ^{26}Ne and has successfully described the PDR, GDR, and their decay patterns [138].

The advantages of the model are as follows. (1) The AMD wave function can describe both the collective states and cluster states, such as α clustering, which is essential for estimating the α-decay branch. (2) Rotational symmetry is restored by the angular momentum projection. This enables us to describe the rotational modes and rotation-vibration coupling in addition to the vibrational modes. (3) The REM handles many-particle-many-hole states, which enables the investigation of many-body correlations beyond the PRA approximation. (4) The decay branches can be reasonably estimated using the Laplace expansion model.

The following issues are planned to be resolved. (1) An effective interaction that reasonably describes the structure and response of the light nuclei needs to be developed because the current Skyrme density functionals do not work well for very light nuclei. (2) This project will be the first application of REM to AMD, and thus computer code development and benchmarking are required.

3.5 Large-scale shell-model (LSSM) calculations

Shell-model calculations are considerably successful in systematically reproducing low-lying states, and can be a promising option for describing photonuclear reactions. The photonuclear reactions introduce a parity change in the excitation from the ground state, demanding significantly larger valence shells. The minimum model space to satisfy the $E1$ sum is the $0\hbar\omega$ space for the ground state and $1\hbar\omega$ space for the $E1$-excited states. In particular, when the Fermi surface is located in the major shell having the harmonic-oscillator quantum number $\mathcal{N}_0\hbar\omega$, three major shells with $(\mathcal{N}_0 - 1)\hbar\omega$, $\mathcal{N}_0\hbar\omega$, and $(\mathcal{N}_0 + 1)\hbar\omega$ have to be considered as the valence shell, and all the possible basis states whose harmonic-oscillator quantum numbers $1\hbar\omega$ have to be considered as larger than the lowest. Such calculations are usually referred to as the $1\hbar\omega$ calculations.

Figure 12 presents the M-scheme basis dimensions for the 1^- states of $N = Z$ even-even nuclei ranging from ^{16}O to ^{56}Ni. The circles denote those of the $1\hbar\omega$ calculations. For the nuclei with $16 < A < 40$, the valence shell consists of $\mathcal{N}_0 = 1, 2, 3$ major shells, and the M-scheme basis dimension peaks at the middle of the sd shell, ^{28}Si. For nuclei with $A > 40$, the valence shell changes to $\mathcal{N}_0 = 2, 3, 4$ major shells. The dimension steeply increases with the mass number than that for $16 < A < 40$, and reaches approximately 10^{11} at ^{56}Ni. Because recent large-scale shell-model codes can handle 10^{10}–10^{11} M-scheme dimensions, w$1\hbar\omega$ calculations can be carried out for almost all the nuclei of interest using the KSHELL code [140].

The next leading order to be included as the basis states are the $3\hbar\omega$ ones. These states consist of (i) one-nucleon excitation to the $3\hbar\omega$ larger shell and (ii) three-nucleon excitations to the $1\hbar\omega$ larger shells. Because the basis states of (i) require

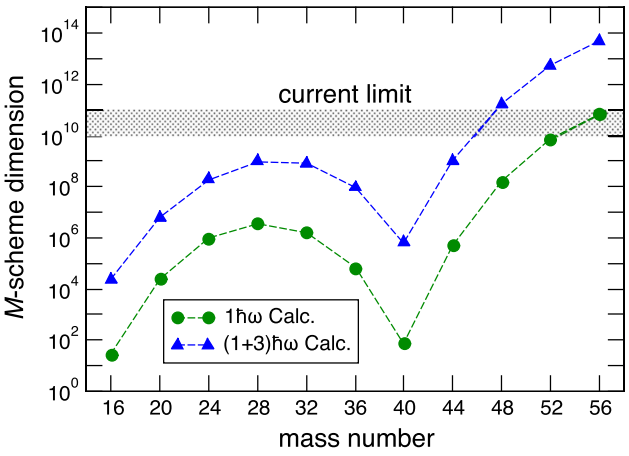

Fig. 12 M-scheme dimensions for the 1^- states of $N = Z$ even-even nuclei

significantly more valence shells beyond the capability of the current version of KSHELL, currently only the basis states of (ii) can be included. We confirmed that the missing $E1$ strengths owing to the lack of (i) are negligible, and such approximate calculations are referred to as $(1 + 3)\hbar\omega$ calculations. As shown in Fig. 12, the $(1 + 3)\hbar\omega$ basis dimensions are ~ 3 orders larger than the $1\hbar\omega$ ones. However, the dimensions of the sd-shell nuclei (i.e., $16 < A < 40$ ones) are still below the considerable limit. The $1\hbar\omega$ and $(1 + 3)\hbar\omega$ calculations are compared in Ref. [27] for ^{48}Ca. While the $E1$ strengths below the GDR peak are approximately the same, those above the GDR peak are reduced in the $(1+3)\hbar\omega$ calculation and appear closer to the experimental data, probably owing to improved correlations. Therefore, we considered that the best strategy for the current study is to carry out $(1 + 3)\hbar\omega$ calculations for the sd-shell and lighter pf-shell nuclei and to perform $1\hbar\omega$ calculations with empirical corrections for higher excitation energies included.

Furthermore, numerical calculations derived from different LSSM codes and interaction schemes can be compared and used for theoretical predictions of nuclear excitations in light nuclei of interest for the present study.

3.6 Ab initio no-core shell model calculation

Recently ab initio studies of the giant dipole resonance were performed in light nuclei, such as ^{4}He [141], ^{10}B, [142] and ^{16}O [143]. In these *ab initio* approaches, one of the most challenging obstacles is to treat the hard-core nature of nuclear forces, which often demands a prohibitively large model space in no-core shell model calculations.

In Ref. [142], no-core shell model calculations successfully described the giant dipole resonance by employing modern chiral N^{3}LO interactions. In this study, similarity-renormalization-group (SRG) evolution was applied to the

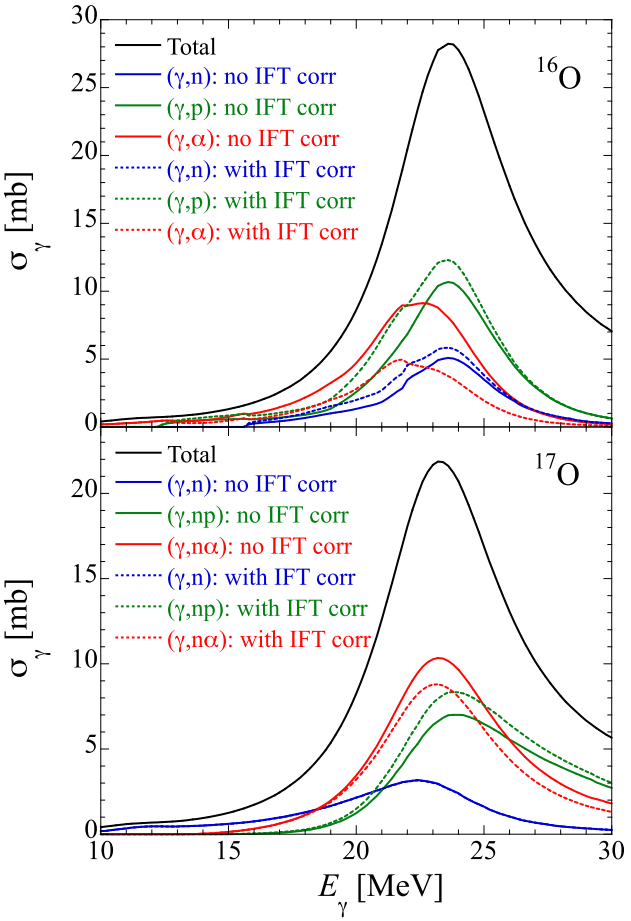

Fig. 13 TALYS prediction of the dominant photoreaction cross sections on ^{16}O and ^{17}O with or without including the IFT corrections

chiral N^{3}LO interaction to soften the hard-core nature of the nuclear force, and it was demonstrated that the giant dipole resonance obtained by the no-core shell model approach converged with a relatively small model space. In this study, we will perform no-core shell model calculations to obtain the giant dipole resonances of light nuclei using other softened interactions, such as the Daejeon 16 interaction [144], employing the KSHELL code [140]. To treat large active shells required in no-core shell model calculations, we may have to develop the KSHELL code further. Moreover, it is desirable to construct an effective $E1$ operator, to which the bare $E1$ operator is renormalized in the model space. In parallel, we will perform no-core shell model calculations employing conventional phenomenological interactions such as the WBT interaction [145] for simplicity and comparison with the ab initio approaches.

4 Reaction calculations

To estimate the photoreaction cross-sections of interest in this study, the different reaction mechanisms had to be simulated. One of the modern reaction codes called TALYS [146] includes many state-of-the-art nuclear models to cover all the main reaction mechanisms encountered in light particle-induced nuclear reactions. It provides a complete description of all the reaction channels and observables. The code includes photons, neutrons, protons, deuterons, tritons, ^{3}He, and α-particles as both projectiles and ejectiles, and single- and multi-particle emissions and fission. All the experimental information on nuclear masses, deformation, and low-lying state spectra is considered, whenever available [147]. If not, various local and global input models have been incorporated to represent the nuclear structure properties, optical potentials, level densities, γ-ray strengths, and fission properties. The TALYS code was designed to calculate the total and partial cross-sections, residual and isomer production cross-sections, discrete and continuum γ-ray production cross-sections, energy spectra, angular distributions, double-differential spectra, and recoil cross-sections. Furthermore, TALYS estimates the thermonuclear reaction rates relevant to astrophysics [148].

The treatment of the photon strength function is particularly relevant to this study. Different models of the dipole strength function are available in TALYS in particular, the Simple Modified Lorentzian model (SMLO) [149], or the Gogny D1M+QRPA model [150], but the experimental strength can also be directly introduced. In addition, for the present project, two recent improvements have been brought to the TALYS code: (i) an updated description of the nuclear level density of light nuclei within the constant-temperature model [151], where the model parameters have been adjusted individually to all light targets of interest in the present project, and (ii) the account of isospin forbidden transitions (IFT) both in the single and multiple particle emission channels. For the latter, a phenomenological correction reflecting the hindrance of dipole emission in self-conjugate nuclei is introduced, as detailed in Ref. [152]. Including IFT corrections can lead to rather different predictions of photoemission cross-sections in targets, such as ^{16}O or ^{17}O, as illustrated in Fig. 13.

Based on the statistical model of Hauser–Feshbach, TALYS is a successful code for medium- and heavy-mass target nuclei. Such a model assumes that the capture process occurs with the intermediary formation of a compound nucleus in thermodynamic equilibrium. The energy of the incident particle is then shared almost uniformly by all the nucleons before releasing the energy through particle emission or γ-de-excitation. The formation of a compound nucleus is generally justified by assuming that the level density in the compound nucleus at the projectile incident energy

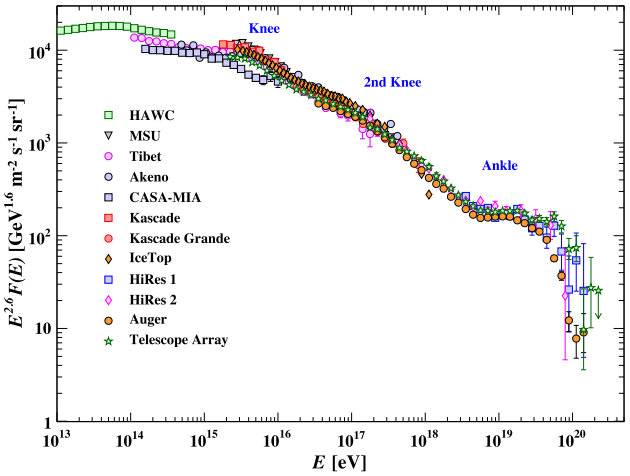

Fig. 14 Observed cosmic-ray flux distribution as a function of the (total) energy [154] above 10 TeV, including data from major UHECR observatories such as Pierre Auger (the orange circles) and Telescope Array (the green stars). A cut-off is visible above a few 10^{19} eV

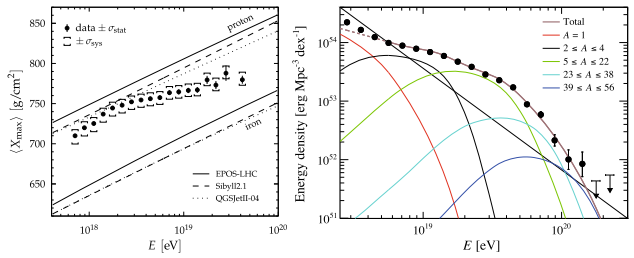

Fig. 15 The atmospheric depth of the maximum air shower, $< X_{\max} >$, as a function of the UHECR energy from the Pierre Auger Observatory in comparison with three model predictions for the cases of primary UHECR particles of protons and irons (left panel) [155]. The observed UHECR flux distribution above 10^{18} eV from the Pierre Auger Observatory compared with an example mass-composition analysis (right panel) [156]

is sufficiently large to ensure an average statistical continuum superposition of the available resonances. However, when the number of available states in the compound system is relatively small, as for light targets, the validity of the Hauser-Feshbach predictions has to be questioned. Therefore, a priori, the statistical model is not well suited for describing the reaction mechanisms occurring with the light species investigated in the current project. However, it appears to provide sufficiently fair rates that can be used as a first estimate for sensitivity analysis and further adjusted in specific cases, as shown in Ref. [153]. As shown in Fig. 13, the IFT corrections can be used to tune the photoreaction cross-sections close to the $N = Z$ line.

5 UHECR physics

5.1 Observations and open questions

Even after more than fifty years of experimental efforts, the origin of UHECRs, the cosmic-rays above 10^{18} eV remains a mystery. Understanding the production of these cosmic rays, which are considered the most energetic particles in the universe, is one of the most intense research fields in high-energy astrophysics. High-resolution and high-statistics measurements of the UHECR spectrum, composition, and arrival direction have recently become possible through experiments, such as AGASA [157], HiRes [158], the Pierre Auger Observatory [159], and Telescope Array (TA) [160], based on the detection of giant air showers triggered by the interaction of UHECRs in the Earth's atmosphere. Evidence of suppression of the UHECR flux above 3–5 $\times$ 10^{19} eV observed by HiRes [161], the Pierre Auger Observatory [162], and TA [163,164] (see Fig. 14) is one of the most anticipated observations at the highest energies. Composition analyses at the Pierre Auger observatory strongly favor a mixed composition with an evolution toward heavier elements (but most probably not heavier than Fe nuclei) above a few 10^{18} eV [155,165,166] (Fig. 15). This quite unexpected trend demonstrates the central importance of complex nuclei ($A = 2$ and heavier) in UHECR physics. In addition, the presence of these complex nuclei shows that UHECRs are accelerated in astrophysical sources rather than being directly produced by exotic high-energy particle physics phenomena. Anisotropies in the arrival directions of UHECRs are additional critical pieces of information that constrain their origins. Recent data have provided the first clear evidence (above the 5σ significance threshold) of large-scale anisotropy (a dipole modulation) in the distribution of the arrival direction of the highest energy events [167]. Moreover, Auger and TA data show hints of anisotropies at smaller angular scales ($\sim$ 20–25°) with claimed excesses in the direction of the Centaurus [168] and Ursa Major [169]. Despite this evidence of anisotropies, the astrophysical production sites of UHECRs remain challenging to trace. This is probably a consequence of the significant angular deflections experienced by UHECRs, owing to the cosmic magnetic fields, during their journey from their sources to the Earth. Nevertheless, these anisotropic observations seem to support the general idea that UHECRs are of extragalactic origin (as already accepted based on simple theoretical considerations).

5.2 Extragalactic propagation of UHECRs

Owing their likely extragalactic origin, the UHECR spectrum and composition measured on Earth must be shaped by the effect of propagation of the particles in the extragalactic medium. During their journey from the sources (expected to be distributed somewhat like ordinary matter throughout the entire universe) to Earth, the injected cosmic-ray spectrum

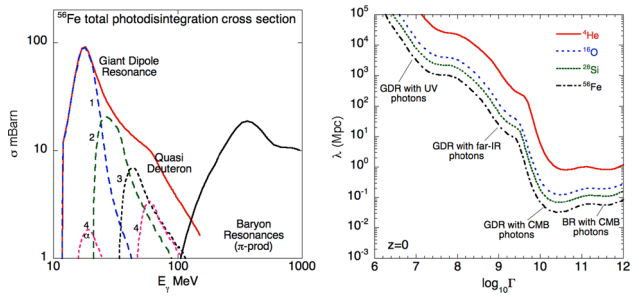

Fig. 16 Left: energy evolution of the photodisintegration cross-section for ^{56}Fe, the contributions of the GDR, quasi-deuteron (QD) and baryon resonances (BR) are shown in addition to the contributions of different nucleon multiplicities (for GDR and QD). The cross-sections in the GDR and QD regimes were obtained using the TALYS code. Right: total photodisintegration mean free path for various species as a function of the Lorentz factor (refer the labels) at redshift $z = 0$ (adapted from [88])

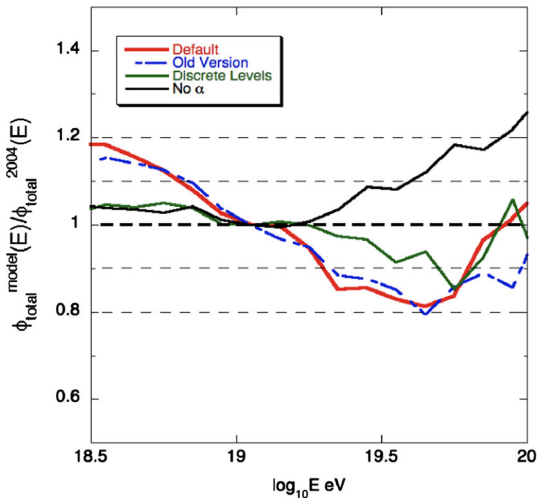

Fig. 17 Illustration of the effect of the α decay channel on the expected flux after propagation in the intergalactic space, assuming a uniform distribution of sources in the universe, for a few different theoretical assumptions on the GDR cross-sections corresponding to the various TALYS settings. The graph shows the relative difference between the predicted UHECR fluxes on Earth as a function of energy for the various assumptions. The flux obtained for the cross-sections of [172] are used as the reference

and mass composition are modified by the interactions of UHECRs with background photons (resulting in energy and mass losses) and cosmic magnetic fields (resulting in deflections). Detailed modeling of the extragalactic propagation of UHECRs is necessary for the astrophysical interpretation of the data. One key feature induced by the UHECRs extragalactic propagation is the prediction of a cut-off in the observed spectrum above a few 10^{19} eV related to the interactions of UHE protons or nuclei with photons from the CMB as well as with infrared, optical, and ultraviolet extragalactic backgrounds (hereafter IR/Opt/UV). This prediction [170,171] of the so-called GZK cut-off (named after the authors of the original studies Greisen, Zatsepin, and Kuzmin) was made in 1966, shortly following the discovery of the CMB, and seems to be consistent with the aforementioned spectral measurements.

Only the photointeractions are relevant in the extragalactic medium, except in the immediate vicinity of the UHECRs acceleration site. The principle of the photo-interactions suffered by the UHECR protons and nuclei during their intergalactic journey, with photon backgrounds of energies ranging from 10^{-3} eV (CMB) to a few eV (UV) in the Earth frame, is relatively simple. Cosmic-ray protons or nuclei with a Lorentz factor large enough would see photons of these low-energy backgrounds as multi-MeV photons in their proper reference frame, that is, above the threshold energies for the e^+e^- pair production or pion production for protons or nucleon separation for complex nuclei. Whenever this occurs, each of these interactions results in energy losses for the incoming ultra-relativistic cosmic rays either by decelerating or losing nucleons. As a result, complex nuclei contained in UHECRs suffer mainly from IVGDR, hereafter more shortly GDR excitations with extra-galactic photons for Lorentz factors above $\sim 10^{8.5}$ with far-infrared photons and $\sim 10^{9.5}$ with CMB photons (see Fig. 16). This results in nucleon losses and modification of the UHECR composition with respect to that produced in the unknown sources. Note that excitation of GDR is the most important photodisintegration process for UHECR nuclei because it has the largest cross-section and lowest energy threshold. Thus it has a dominant contribution to the UHECR nuclei with a photodisintegration mean free path for the Lorentz factor ranging from $\sim 10^7$ to 10^{11} (Fig. 16).

The most significant early study of UHECR nuclei propagation was certainly performed by Puget, Stecker, and Bredekamp (PSB) [173], who treated, in great detail, the propagation of nuclei ($A \leq 56$) and provided simple parametrizations based on the available data for the GDR and quasi-deuteron (QD) excitation cross sections. More recently, Khan et al. [172] proposed new estimates of the GDR cross-section based on a theoretical calculation using the TALYS nuclear reaction code [89], which showed better agreement with the available data than that with the previous parametrizations from PSB [173]. The improvement in the UHECR estimates owing to these new calculations rely not only on the use of microscopic cross sections but also on the implementation of a photodisintegration network involving many nuclei in contrast to the previous methodology, where only one given nucleus was considered for each A below 56.

In recent years, the interest in the propagation of UHECR nuclei has increased significantly (Ref. [88] for recent review and references therein). This further holds because the recent composition analyses at the Pierre Auger Observatory now firmly indicate a significant (and increasing with energy) con-

tribution of nuclei at the highest energies. The availability of GDR cross-section models, as well constrained and as realistic as possible, is critical for obtaining the most information from extragalactic UHECR propagation studies. In some predictions of nuclear reaction codes, such as TALYS (see the previous sections), for instance, the importance of the α-decay reaction channels for low-mass nuclei, depend on the chosen settings of nuclear reaction code and are, contrarily, not ell constrained currently by nuclear physics measurements. The latitude left by the lack of experimental constraints, together with the dependence on the nuclear reaction code settings, can lead to a sizeable dispersion of the predicted UHECR spectrum after accounting for the UHECR extragalactic propagation for a given source spectrum and composition model as illustrated in Fig. 17. The dispersion of the UHECR spectrum was also evaluated in Ref. [174] using the RPA-EDF model [24,175] with several Skyrme-EDF parameters.

An exhaustive campaign of measurements of GDR cross-sections for various nuclei and reaction channels, as proposed in the PANDORA framework could significantly improve the description of nuclear reactions relevant to the propagation of UHECRs. Likewise, these improvements would also benefit the modeling of UHECR acceleration in potential UHECR astrophysical sources, including active galactic nuclei [176–181], gamma-ray bursts [182–185], star-burst galaxies [186–188], galaxy clusters [189–191], or tidal disruption events [192], where photo interactions could also play an important role.

6 Applications

6.1 Astrophysical applications beyond UHECRs

In addition to their relevance to a proper understanding of the UHECR composition and energy spectrum as detected on Earth (Sect. 5), photoreactions play an important role in stellar evolution and nucleosynthesis applications [193]. More specifically, at high temperatures (typically in excess of 10^9K), nuclei may be subject to (γ, n), (γ, p) or (γ, α) photodisintegration. These transformations have become increasingly important as the evolution of a star proceeds beyond C-burning in the non-explosive history of massive stars. The first major stage of photodisintegrations is the Ne-burning episode governed by the $^{20}\mathrm{Ne}(\gamma, \alpha)^{16}\mathrm{O}$ reaction, which also produces a significant amount of recaptured α-particles responsible for the production of elements heavier than Ne. Photodisintegration culminates at the Si-burning phase, terminating at a nuclear statistical equilibrium. Explosive situations favor photodisintegrations owing to the higher temperatures reached under these conditions. Notably, some occur during the various hot modes of H-burning [194] and are essential components of the $p-$ and $r-$ processes of nucleosynthesis [195,196].

The photodisintegration rates in a photon bath obeying the Plank distribution law that applies to stellar interiors are briefly discussed in Ref. [194]. In view of the difficulties in deriving photodisintegration rates through direct approaches, they have traditionally been estimated based on the detailed balance theorem applicable to the reverse radiative capture of nucleons or α-particles (e.g. [152,194]). However, photoreaction experiments can be of great interest to constrain the reverse cross-sections, especially when dealing with an unstable target in radiative capture, which cannot be measured in the laboratory. For example, the photodisintegration of ^{9}Be through the $1/2^+$ state near the neutron threshold [197] helped to constrain the important three-body inverse reaction ($\alpha\alpha$n) of relevance during nucleosynthesis in the neutron-rich ν-driven wind of Type-II supernovae.

6.2 Application to other fields

Precise knowledge of the $E1$ transition strength distribution and decay processes is essential for various applications related to γ-ray irradiation and photoexcitation. The excitation-energy distribution of the $E1$ transition strength determines the photoabsorption cross sections and, thus, the reaction rate under γ-ray irradiation. Reliable predictions of the decay processes are indispensable for simulating radiation effects, e.g. the number of nuclei produced after photoexcitation, energy dissipated by the emitted charged particles, amount of neutron radiations produced and the activation by neutrons, production of radioactivity, and emission of characteristic γ-rays used for elemental or isotopic analysis. The photonuclear reaction data and predictions of light nuclei are briefly summarized as follows.

The photonuclear reaction data are essential inputs for the simulation of radiation shielding design, radiation transport analysis, and estimation of radioactivity for decommissioning at industrial, scientific, and medical facilities.

The photon activation analysis (PAA) method has been developed for the non-destructive identification of nuclides in a sample material by detecting the induced radioactivity after exposure to high-energy photons [198]. PAA is more suitable than neutron activation analysis (NAA) for detecting light elements, such as Be, C, N, O, F, Si, P, and Ni [199]. Super-intense Laser-driven photon activation analysis is proposed using photons produced by high-power laser irradiation of a solid material [200]. Gamma-ray imaging by combining the techniques of nuclear resonance fluorescence (NRF) spectroscopy with computer tomography (CT) has been developed for the non-destructive investigation of the distribution of specific isotopes in a material [201].

The inspection of fissile materials by applying photonuclear reactions has been discussed in several studies on inter-

national safeguards and security [202–204]. Although the photo-neutron response of fissile heavy elements is beyond the scope of this study, the photo-neutron response of the surrounding materials, such as the $^{18}O(\gamma, n)$ reaction, needs to be evaluated because the reactions produce noise signals for the detection of the target material [203]. In addition, photoneutron spectroscopy using monoenergetic γ-rays for detecting bulk explosives was studied by measuring the spectrum of emitted characteristic neutrons to identify nuclei associated with the explosives (H, C, N, O) [205]

The production of medical isotopes through photon irradiation was investigated for ^{44}Sc and ^{47}Ca via (γ, n), ^{47}Sc voa (γ, p), and ^{44}Ti via $(\gamma, 2n)$ reactions [206]. Precise data on photonuclear reactions on elements of the human body are essential for simulating the absorbed doses during radiotherapy.

Recently, photonuclear reactions triggered by lightning discharge were observed using terrestrial scintillation γ detectors [207,208]. However, the ignition process and lightning discharge development are still poorly understood. The accelerated electrons in the thundercloud emit γ rays by bremsstrahlung, which produce ^{13}N and ^{15}O nuclei via $^{14}N(\gamma, n)$ and $^{16}O(\gamma, n)$ reactions in the atmosphere. The produced nuclei emit positrons with half-lives of several minutes. The annihilation γ-rays are observed using scintillation γ-detectors. Precise knowledge of the photonuclear reactions on the relevant nuclides is required to describe the lightning mechanism in thunderclouds before and after discharge.

7 Summary and outlook

Photonuclear reactions of light nuclei below a mass of $A = 60$ are essential for the nuclear structure and reaction studies, particle and nuclear astrophysics, and various other applications. The PANDORA project aims to systematically investigate the photonuclear reactions, and comprises experimental nuclear physics, theoretical nuclear physics, and particle astrophysics. Two modern experimental methods, virtual photon excitation through proton scattering and real photo absorption using a high-brilliance γ-ray beam produced by laser Compton scattering, will be applied to measure the photoabsorption cross-sections and decay branching ratio of each decay channel. Several nuclear models, such as antisymmetrized molecular dynamics, mean-field and beyond-mean-field models, a large-scale shell model, and ab initio no-core shell model will be employed to predict photonuclear reactions. Uncertainties in the model predictions will also be studied. The results will be implemented in the reaction calculation code TALYS for application in various fields. The photodisintegration process of ultra-high-energy cosmic rays in inter-galactic propagation using the theoretical predictions and uncertainty originating from the accuracy of the nuclear model predictions are the focus of the PANDORA project.

The first beamtimes of the project's nuclear physics experiments are planned for 2023 at the RCNP and iThemba LABS. The first commissioning of the LCS γ-ray facility at the ELI-NP is expected at the end of the year 2023. Systematic data will be obtained in 5–10 years. Simultaneously, the development of nuclear models [91] and their application to UHECR propagation simulations [174] are ongoing. We note that an experimental study on photoneutron cross sections on ^{13}C measured at New SUBARU has been reported [209] after the first submission of this manuscript.

Acknowledgements This work is supported partly by Grants-in-Aid for Scientific Research "KAKENHI" in Japan with grant numbers of JP19H00693 and 22K18715, Japan-South Africa Bilateral Funding from JSPS with a grant number of JPJSBP 120216502 and from NRF with grant number 132993, the National Research Foundation of South Africa through Grants No. 129411, 85509, and 118846, grants of the Romanian Ministry of Research, Innovation and Digitization, CNCS - UEFISCDI, project number PN-III-P4-PCE-2021-0595, within PNCDI III, and the contract PN 23 21 01 06, Pioneering Program of RIKEN for Evolution of Matter in the Universe (r-EMU), and Interdisciplinary Theoretical and Mathematical Sciences program (iTHEMS, https://ithems.riken.jp) at RIKEN, the Deutsche Forschungsgemeinschaft (DFG, German Research Foundation) – Project-ID 279384907 – SFB1245, the State of Hesse within the Research Cluster ELEMENTS (Project ID 500/10.006), the grant "Nuclear Photonics" within the LOEWE program, and EXC-2094 – 390783311 under Germany's Excellence Strategy. S.G. acknowledges financial support from the F.R.S.-FNRS (Belgium). E.L. acknowledges funding from the US-NSF CAREER Grant PHY-1654379 and US-NSF Grant PHY-2209376. Z.Y. acknowledges the support from the National Key R&D Program of China (Grant Nos. 2023YFE0101500, 2022YFA1605100) and the National Natural Science Foundation of China (Grant No. 12275006).

Funding Open access funding provided by Osaka University.

Data Availability This manuscript has no associated data or the data will not be deposited. [Authors' comment: All the experimental data in this article are already published.]

References

1. A. Bracco, E. Lanza, A. Tamii, Prog. Part. Nucl. Phys. **106**, 360 (2019)

2. A. Zilges, D. Balabanski, J. Isaak, N. Pietralla, Prog. Part. Nucl. Phys. **122**, 103903 (2022)
3. D. Savran, T. Aumann, A. Zilges, Prog. Part. Nucl. Phys. **70**, 210 (2013)
4. X. Roca-Maza, N. Paar, Prog. Part. Nucl. Phys. **101**, 96 (2018)
5. P. von Neumann-Cosel, A. Tamii, Eur. Phys. J. A **55**, 110 (2019)
6. A. Tamii, I. Poltoratska, P. von Neumann-Cosel, Y. Fujita, T. Adachi, C.A. Bertulani, J. Carter, M. Dozono, H. Fujita, K. Fujita et al., Phys. Rev. Lett. **107**, 062502 (2011)
7. X. Roca-Maza, X. Viñas, M. Centelles, B.K. Agrawal, G. Colò, N. Paar, J. Piekarewicz, D. Vretenar, Phys. Rev. C **92**, 064304 (2015)
8. D. Brink, Ph.D. thesis, University of Oxford (1955)
9. P. Axel, Phys. Rev. **126**, 671 (1962)
10. S. Goriely, Phys. Lett. B **436**, 10 (1998)
11. N. Otuka, E. Dupont, V. Semkova, B. Pritychenko, A. Blokhin, M. Aikawa, S. Babykina, M. Bossant, G. Chen, S. Dunaeva et al., Nucl. Data Sheets **120**, 272 (2014). https://www-nds.iaea.org/exfor/
12. K. Maeda, S. Ito, H. Itoh, O. Konno, H. Matsuyama, T. Murakami, T. Sasaki, T. Suda, M. Takeya, T. Terasawa, J. Phys. Soc. Jpn. **75**, 034201 (2006)
13. R. Koch, H. Thies, Nucl. Phys. A **272**, 296 (1976)
14. J. Jury, B. Berman, D. Faul, P. Meyer, K. McNeill, J. Woodworth, Phys. Rev. C **19**, 1684 (1979)
15. M. Freer, H. Horiuchi, Y. Kanada-En'yo, D. Lee, U.G. Meißner, Rev. Mod. Phys. **90**, 035004 (2018)
16. B.N. Lu, N. Li, S. Elhatisari, Y.Z. Ma, D. Lee, U.G. Meißner, Phys. Rev. Lett. **128**, 242501 (2022)
17. R. Bijker, F. Iachello, Nucl. Phys. A **957**, 154 (2017)
18. R. Bijker, F. Iachello, Prog. Part. Nucl. Phys. **110**, 103735 (2020)
19. M. Kimura, T. Suhara, Y. Kanada-En'yo, Eur. Phys. J. A **52**, 373 (2016)
20. Y. Taniguchi, M. Kimura, H. Horiuchi, Prog. Theor. Phys. **112**, 475 (2004)
21. E. Litvinova, P. Ring, V. Tselyaev, Phys. Rev. C **78**, 014312 (2008)
22. E. Litvinova, P. Ring, V. Tselyaev, Phys. Rev. Lett. **105**, 022502 (2010)
23. C. Robin, E. Litvinova, Eur. Phys. J. A **52**, 205 (2016)
24. T. Inakura, T. Nakatsukasa, K. Yabana, Phys. Rev. C **84**, 021302 (2011)
25. N. Tsoneva, H. Lenske, C. Stoyanov, Phys. Lett. B **586**, 213 (2004)
26. N. Tsoneva, H. Lenske, Phys. At. Nucl. **79**, 885 (2016)
27. Y. Utsuno, N. Shimizu, T. Otsuka, S. Ebata, M. Honma, Prog. Nucl. Energy **82**, 102 (2015)
28. A. Tamii et al., Nucl. Instrum. Methods Phys. Res. A **605**, 326 (2009)
29. R. Neveling et al., Nucl. Instrum. Methods Phys. Res. A **654**, 29 (2011)
30. S. Gales, D.L. Balabanski, F. Negoita, O. Tesileanu, C.A. Ur, D. Ursescu, N.V. Zamfir, Phys. Scr. **91**, 093004 (2016)
31. H. Toyokawa, H. Ohgaki, S. Sugiyama, T. Mikado, K. Yamada, N. Sei, R. Suzuki, T. Ohdaira, T. Yamazaki, Nucl. Instrum. Methods Phys. Res. A **422**, 95 (1999)
32. T. Kawano, Y. Cho, P. Dimitriou, D. Filipescu, N. Iwamoto, V. Plujko, X. Tao, H. Utsunomiya, V. Varlamov, R. Xu et al., Nucl. Data Sheets **163**, 109 (2020)
33. N. Pietralla, H. Weller, V. Litvinenko, M. Ahmed, A. Tonchev, Nucl. Instrum. Methods Phys. Res. A **483**, 556 (2002)
34. J. Ahrens et al., Nucl. Phys. A **251**, 479 (1975)
35. M. Gai et al., The structure of l2C and stellar helium burning. J. Phys. Conf. Ser. **267**, 012046 (2011)
36. W. Zimmerman, M. Ahmed, B. Bromberger, S. Stave, A. Breskin, V. Dangendorf, T. Delbar, M. Gai, S. Henshaw, J. Mueller et al., Phys. Rev. Lett. **110**, 152502 (2013)
37. J. Mueller, M. Ahmed, B. Davis, H. Karwowski, D. Markoff, L. Myers, M. Spraker, S. Stave, J. Tompkins, H. Weller et al., Phys. Rev. C **92**, 034604 (2015)
38. M. Fujiwara, H. Akimune, I. Daito, H. Fujimura, Y. Fujita, K. Hatanaka, H. Ikegami, I. Katayama, K. Nagayama, N. Matsuoka et al., Nucl. Instrum. Methods Phys. Res. A **422**, 484 (1999)
39. P. von Neumann-Cosel, A. Tamii, Eur. Phys. J. A **55**, 110 (2019)
40. N. Kobayashi, K. Miki, T. Hashimoto, C. Iwamoto, A. Tamii, N. Aoi, M. Carpenter, K. Hatanaka, J. Isaak, E. Ideguchi et al., Eur. Phys. J. A **55**, 231 (2019)
41. Y. Fujikawa, K. Sakanashi, S. Adachi, T. Kawabata, T.F. et al., Private communication; candidates for the 5α condensed state in ^{20}Ne in RCNP Annual Report 2021 Highlights (2021). https://www.rcnp.osaka-u.ac.jp/~annurep/2021/
42. A. Giaz, L. Pellegri, S. Riboldi, F. Camera, N. Blasi, C. Boiano, A. Bracco, S. Brambilla, S. Ceruti, S. Coelli et al., Nucl. Instrum. Methods Phys. Res. A **729**, 910 (2013)
43. G. Gosta, N. Blasi, F. Camera, B. Million, A. Giaz, O. Wieland, F. Rossi, H. Utsunomiya, T. Ari-izumi, D. Takenaka et al., Nucl. Instrum. Methods Phys. Res. A **879**, 92 (2018)
44. P. Adsley, R. Neveling, P. Papka, Z. Dyers, J.W. Brümmer, C.A. Diget, N.J. Hubbard, K.C.W. Li, A. Long, D.J. Marin-Lambarri et al., J. Instrum. **12**, T02004 (2017)
45. S. Gales, K.A. Tanaka, D.L. Balabanski, F. Negoita, D. Stutman, O. Tesileanu, C.A. Ur, D. Ursescu, I. Andrei, S. Ataman et al., Rep. Prog. Phys. **81**, 094301 (2018)
46. K.A. Tanaka, K.M. Spohr, D.L. Balabanski, S. Balascuta, L. Capponi, M.O. Cernaianu, M. Cuciuc, A. Cucoanes, I. Dancus, A. Dhal et al., Matter Radiat. Extremes **5**, 024402 (2020)
47. F. Lureau, G. Matras, O. Chalus, C. Derycke, T. Morbieu, C. Radier, O. Casagrande, S. Laux, S. Ricaud, G. Rey et al., High Power Laser Sci. Eng. **8**, e43 (2020)
48. F. Camera, H. Utsunomiya, V. Varlamov, D. Filipescu, V. Baran, A. Bracco, G. Colo, I. Gheorghe, T. Glodariu, C. Matei et al., Rom. Rep. Phys. **68**, S539 (2016)
49. M. Krzysiek, F. Camera, D.M. Filipescu, H. Utsunomiya, G. Colò, I. Gheorghe, Y. Niu, Nucl. Instrum. Methods Phys. Res. A **916**, 257 (2019)
50. P.A. Söderström, E. Açıksöz, D.L. Balabanski, F. Camera, L. Capponi, G. Ciocan, M. Cuciuc, D.M. Filipescu, I. Gheorghe, T. Glodariu et al., Nucl. Instrum. Methods Phys. Res. A **1027**, 166171 (2022)
51. B.L. Berman, S.C. Fultz, Rev. Mod. Phys. **47**, 713 (1975)
52. I. Gheorghe, H. Utsunomiya, S. Katayama, D. Filipescu, S. Belyshev, K. Stopani, V. Orlin, V. Varlamov, T. Shima, S. Amano et al., Phys. Rev. C **96**, 044604 (2017)
53. H. Utsunomiya, I. Gheorghe, D.M. Filipescu, T. Glodariu, S. Belyshev, K. Stopani, V. Varlamov, B. Ishkhanov, S. Katayama, D. Takenaka et al., Nucl. Instrum. Methods Phys. Res. A **871**, 135 (2017)
54. I. Gheorghe, H. Utsunomiya, K. Stopani, D. Filipescu, T. Ari-izumi, S. Belyshev, G. Fan, M. Krzysiek, L. Liu, Y.W. Lui et al., Nucl. Instrum. Methods Phys. Res. A **1019**, 165867 (2021)
55. O. Tesileanu, M. Gai, A. Anzalone, C. Balan, J.S. Bihalowicz, M. Cwiok, W. Dominik, S. Gales, D.G. Ghita, Z. Janas et al., Rom. Rep. Phys. **68**, S699 (2016)
56. S. Chesnevskaya, D. Balabanski, D. Choudhury, P. Constantin, D. Filipescu, D. Ghita, G. Guardo, D. Lattuada, C. Matei, A. Rotaru et al., J. Instrum. **13**, T05006 (2018)
57. H.R. Weller, M.W. Ahmed, H. Gao, W. Tornow, Y.K. Wu, M. Gai, R. Miskimen, Prog. Part. Nucl. Phys. **62**, 257 (2009)
58. B. Löher, V. Derya, T. Aumann, J. Beller, N. Cooper, M. Duchene, J. Endres, E. Fiori, J. Isaak, J. Kelley et al., Nucl. Instrum. Methods Phys. Res. A **723**, 136 (2013)

59. N. Pietralla, Z. Berant, V.N. Litvinenko, S. Hartman, F.F. Mikhailov, I.V. Pinayev, G. Swift, M.W. Ahmed, J.H. Kelley, S.O. Nelson et al., Phys. Rev. Lett. **88**, 012502 (2002)
60. J. Isaak, D. Savran, M. Fritzsche, D. Galaviz, T. Hartmann, S. Kamerdzhiev, J.H. Kelley, E. Kwan, N. Pietralla, C. Romig et al., Phys. Rev. C **83**, 034304 (2011)
61. P.M. Goddard, N. Cooper, V. Werner, G. Rusev, P.D. Stevenson, A. Rios, C. Bernards, A. Chakraborty, B.P. Crider, J. Glorius et al., Phys. Rev. C **88**, 064308 (2013)
62. R. Schwengner, R. Massarczyk, M. Scheck, W. Tornow, G. Battaglia, T. Beck, D. Bemmerer, N. Benouaret, R. Beyer, M. Butterling et al., Phys. Rev. C **103**, 024312 (2021)
63. T. Beck, J. Beller, N. Pietralla, M. Bhike, J. Birkhan, V. Derya, U. Gayer, A. Hennig, J. Isaak, B. Löher et al., Phys. Rev. Lett. **118**, 212502 (2017)
64. T. Beck, V. Werner, N. Pietralla, M. Bhike, N. Cooper, U. Friman-Gayer, J. Isaak, R.V. Jolos, J. Kleemann, Krishichayan et al., Phys. Rev. Lett. **125**, 092501 (2020)
65. K.E. Ide, T. Beck, V. Werner, M. Berger, S.W. Finch, U. Friman-Gayer, J. Kleemann, Krishichayan, B. Löher, O. Papst et al., Phys. Rev. C **103**, 054302 (2021)
66. J. Kleemann, T. Beck, U. Friman-Gayer, N. Pietralla, V. Werner, S.W. Finch, J. Kotila, Krishichayan, B. Löher, H. Pai et al., Phys. Rev. C **104**, L061302 (2021)
67. A.P. Tonchev, S.L. Hammond, J.H. Kelley, E. Kwan, H. Lenske, G. Rusev, W. Tornow, N. Tsoneva, Phys. Rev. Lett. **104**, 072501 (2010)
68. B. Löher, D. Savran, T. Aumann, J. Beller, M. Bhike, N. Cooper, V. Derya, M. Duchêne, J. Endres, A. Hennig et al., Phys. Lett. B **756**, 72 (2016)
69. J. Isaak, D. Savran, M. Krticka, M.W. Ahmed, J. Beller, E. Fiori, J. Glorius, J.H. Kelley, B. Löher, N. Pietralla et al., Phys. Lett. B **727**, 361 (2013)
70. J. Isaak, D. Savran, B. Löher, T. Beck, U. Friman-Gayer, Krishichayan, N. Pietralla, V.Y. Ponomarev, M. Scheck, W. Tornow et al., Phys. Rev. C **103**, 044317 (2021)
71. J. Isaak, D. Savran, B. Löher, T. Beck, M. Bhike, U. Gayer, Krishichayan, N. Pietralla, M. Scheck, W. Tornow et al., Phys. Lett. B **788**, 225 (2019)
72. O. Papst, V. Werner, J. Isaak, N. Pietralla, T. Beck, C. Bernards, M. Bhike, N. Cooper, B.P. Crider, U. Friman-Gayer et al., Phys. Rev. C **102**, 034323 (2020)
73. W. Tornow, V.N. Litvinenko, A. Hutcheson, N.G. Czakon, C.R. Howell, G.J. Weisel, S. Mikhailov, I.V. Pinayev, J.H. Kelley, H. Witala, Phys. Lett. B **574**, 8 (2003)
74. M.W. Ahmed, M.A. Blackston, B.A. Perdue, W. Tornow, H.R. Weller, B. Norum, B. Sawatzky, R.M. Prior, M.C. Spraker, Phys. Rev. C **77**, 044005 (2008)
75. W.R. Zimmerman, M.W. Ahmed, B. Bromberger, S.C. Stave, A. Breskin, V. Dangendorf, T. Delbar, M. Gai, S.S. Henshaw, J.M. Mueller et al., Phys. Rev. Lett. **110**, 152502 (2013)
76. M. Scheck, V.Y. Ponomarev, T. Aumann, J. Beller, M. Fritzsche, J. Isaak, J.H. Kelley, E. Kwan, N. Pietralla, R. Raut et al., Phys. Rev. C **87**, 051304 (2013)
77. R. Schwengner, R. Massarczyk, R. Beyer, M. Bhike, B.A. Brown, Krishichayan, K. Sieja, W. Tornow, D. Bemmerer, M. Butterling et al., Phys. Rev. C **101**, 064303 (2020)
78. J. Kleemann, Technical University of Darmstadt, Institute for Nuclear Physics, private communication (2022)
79. A. Zilges, D. Balabanski, J. Isaak, N. Pietralla, Prog. Part. Nucl. Phys. **122**, 103903 (2022)
80. D. Savran, K. Lindenberg, J. Glorius, B. Löher, S. Müller, N. Pietralla, L. Schnorrenberger, V. Simon, K. Sonnabend, C. Wälzlein et al., Nucl. Instrum. Methods Phys. Res. A **613**, 232 (2010)
81. N. Pietralla, Nucl. Phys. News **28**, 4 (2018). https://doi.org/10.1080/10619127.2018.1463013
82. H.W. Wang, G.T. Fan, L.X. Liu, H.H. Xu, W.Q. Shen, Y.G. Ma, H. Utsunomiya, L.L. Song, X.G. Cao, Z.R. Hao et al., Nucl. Sci. Technol. **33**, 87 (2022)
83. H. Xu, G. Fan, H. Wang, H. Utsunomiya, L. Liu, Z. Hao, H. Wu, L. Song, Q. Zhang, B. Jiang et al., Nucl. Instrum. Methods Phys. Res. A **1033**, 166742 (2022)
84. Z. Hao, G. Fan, H. Wang, L. Liu, H. Xu, H. Utsunomiya, X. Cao, B. Xu, L. Song, X. Hu et al., Nucl. Instrum. Methods Phys. Res. A **1013**, 165638 (2021)
85. M. Wakasugi, T. Suda, Y. Yano, Nucl. Instrum. Methods **532** (2004)
86. K. Tsukada, A. Enokizono, T. Ohnishi, K. Adachi, T. Fujita, M. Hara, M. Hori, T. Hori, S. Ichikawa, K. Kurita et al., Phys. Rev. Lett. **118**, 1 (2017). arXiv:1703.04278
87. T. Suda, H. Simon, Prog. Part. Nucl. Phys. **96**, 1 (2017)
88. D. Allard, Astropart. Phys. **39**, 33 (2012)
89. A.J. Koning, S. Hilaire, M. Duijvestijn, TALYS: a nuclear reaction program (2004). http//www.talys.eu
90. P. Ring, P. Schuck, *The Nuclear Many-Body Problem* (Springer, Berlin, 1980)
91. T. Inakura (2022), arXiv: 2205.12671 [nucl-th]
92. E. Litvinova, P. Ring, Phys. Rev. C **73**, 044328 (2006)
93. E. Litvinova, P. Ring, V. Tselyaev, Phys. Rev. C **75**, 064308 (2007)
94. E. Litvinova, P. Ring, V. Tselyaev, Phys. Rev. C **78**, 014312 (2008)
95. E. Litvinova, P. Ring, V. Tselyaev, Phys. Rev. Lett. **105**, 022502 (2010)
96. E. Litvinova, Phys. Rev. C **91**, 034332 (2015)
97. C. Robin, E. Litvinova, Eur. Phys. J. A **52**, 205 (2016)
98. C. Robin, E. Litvinova, Phys. Rev. Lett. **123**, 202501 (2019)
99. J. Boguta, A. Bodmer, Nucl. Phys. A **292**, 413 (1977)
100. B.D. Serot, J. Walecka, Phys. Lett. B **87**, 172 (1979)
101. B.D. Serot, J.D. Walecka, Adv. Nucl. Phys. **16**, 1 (1986)
102. B.D. Serot, J.D. Walecka, Int. J. Mod. Phys. E **6**, 515 (1997)
103. P. Ring, Prog. Part. Nucl. Phys. **37**, 193 (1996)
104. P. Ring, Z.Y. Ma, N. Van Giai, D. Vretenar, A. Wandelt, L.G. Cao, Nucl. Phys. A **694**, 249 (2001)
105. D. Vretenar, A.V. Afanasjev, G.A. Lalazissis, P. Ring, Phys. Rep. **409**, 101 (2005)
106. H. Liang, N. Van Giai, J. Meng, Phys. Rev. Lett. **101**, 122502 (2008)
107. N. Paar, P. Ring, T. Nikšić, D. Vretenar, Phys. Rev. C **67**, 034312 (2003)
108. N. Paar, T. Nikšić, D. Vretenar, P. Ring, Phys. Rev. C **69**, 054303 (2004)
109. E. Litvinova, Phys. Lett. B **755**, 138 (2016)
110. D. Bes, R. Broglia, G. Dussel, R. Liotta, R. Perazzo, Nucl. Phys. A **260**, 77 (1976)
111. P.F. Bortignon, R. Broglia, D. Bes, R. Liotta, Phys. Rep. **30**, 305 (1977)
112. G. Bertsch, P. Bortignon, R. Broglia, Rev. Mod. Phys. **55**, 287 (1983)
113. C. Mahaux, P. Bortignon, R. Broglia, C. Dasso, Phys. Rep. **120**, 1 (1985)
114. G. Colò, P.F. Bortignon, Nucl. Phys. A **696**, 427 (2001)
115. Y. Niu, G. Colò, E. Vigezzi, Phys. Rev. C **90**, 054328 (2014)
116. Y. Niu, Z. Niu, G. Colò, E. Vigezzi, Phys. Rev. Lett. **114**, 142501 (2015)
117. S.P. Kamerdzhiev, G.Y. Tertychny, V.I. Tselyaev, Phys. Part. Nucl. **28**, 134 (1997)
118. S. Kamerdzhiev, J. Speth, G. Tertychny, Phys. Rep. **393**, 1 (2004)
119. E. Litvinova, Phys. Rev. C **85**, 021303 (2012)
120. C. Robin, E. Litvinova, Phys. Rev. C **98**, 051301(R) (2018)
121. E. Litvinova, H. Wibowo, Eur. Phys. J. A **55**, 223 (2019)
122. E. Litvinova, C. Robin, H. Wibowo, Phys. Lett. B **800**, 135134 (2020)

123. T. Marketin, E. Litvinova, D. Vretenar, P. Ring, Phys. Lett. B **706**, 477 (2012)
124. E. Litvinova, B. Brown, D.L. Fang, T. Marketin, R. Zegers, Phys. Lett. B **730**, 307 (2014)
125. J. Endres, E. Litvinova, D. Savran, P.A. Butler, M.N. Harakeh, S. Harissopulos, R.D. Herzberg, R. Krücken, A. Lagoyannis, N. Pietralla et al., Phys. Rev. Lett. **105**, 212503 (2010)
126. E. Litvinova, P. Schuck, Phys. Rev. C **100**, 064320 (2019)
127. E.V. Litvinova, A.V. Afanasjev, Phys. Rev. C **84**, 014305 (2011)
128. N. Tsoneva, H. Lenske, Phys. Rev. C **77**, 024321 (2008)
129. V.G. Soloviev, *Theory of Complex Nuclei* (Pergamon Press, Oxford, 1976)
130. A. Tonchev, N. Tsoneva, C. Bhatia, C. Arnold, S.H.S. Goriely, J. Kelley, H.L.E. Kwan, J. Piekarewicz, G.R.R. Raut, T. Shizuma et al., Phys. Lett. B **773**, 20 (2017)
131. M. Spieker, A. Heusler, B.A. Brown, T. Faestermann, R. Hertenberger, G. Potel, M. Scheck, N. Tsoneva, M. Weinert, H.F. Wirth et al., Phys. Rev. Lett. **125**, 102503 (2020)
132. M. Weinert, M. Spieker, G. Potel, N. Tsoneva, M. Müscher, J. Wilhelmy, A. Zilges, Phys. Rev. Lett. **127**, 242501 (2021)
133. N. Tsoneva, H. Lenske, Phys. Lett. B **695**, 174 (2011)
134. N. Tsoneva, M. Spieker, H. Lenske, A. Zilges, Nucl. Phys. A **990**, 183 (2019)
135. R. Raut, A.P. Tonchev, G. Rusev, W. Tornow, C. Iliadis, M. Lugaro, J. Buntain, S. Goriely, J.H. Kelley, R. Schwengner et al., Phys. Rev. Lett. **111**, 112501 (2013)
136. N. Tsoneva, S. Goriely, H. Lenske, R. Schwengner, Phys. Rev. C **91**, 044328 (2015)
137. M. Kimura, Phys. Rev. C **95**, 034331 (2017)
138. R. Imai, T. Tada, M. Kimura, Phys. Rev. C **99**, 064327 (2019)
139. Y. Chiba, M. Kimura, Prog. Theor. Exp. Phys. **2017** (2017)
140. N. Shimizu, T. Mizusaki, Y. Utsuno, Y. Tsunoda, Comput. Phys. Commun. **244**, 372 (2019)
141. W. Horiuchi, Y. Suzuki, K. Arai, Phys. Rev. C **85**, 054002 (2012)
142. M. Kruse, W. Ormand, C. Johnson, Eur. Phys. J. A **55**, 1 (2019)
143. S. Bacca, N. Barnea, G. Hagen, G. Orlandini, T. Papenbrock, Phys. Rev. Lett. **111**, 122502 (2013)
144. A. Shirokov, I. Shin, Y. Kim, M. Sosonkina, P. Maris, J. Vary, Phys. Lett. B **761**, 87 (2016)
145. E.K. Warburton, B.A. Brown, Phys. Rev. C **46**, 923 (1992)
146. A.J. Koning, S. Hilaire, S. Goriely, Eur. Phys. J. A **59**, 131 (2023)
147. R. Capote, M. Herman, P. Oblozinsky, P. Young, S. Goriely, T. Belgya, A. Ignatyuk, A. Koning, S. Hilaire, V. Plujko et al., Nucl. Data Sheets **110**, 3107 (2009)
148. S. Goriely, S. Hilaire, A.J. Koning, A&A **487**, 767 (2008)
149. S. Goriely, S. Hilaire, S. Péru, K. Sieja, Phys. Rev. C **98**, 014327 (2018)
150. S. Goriely, V. Plujko, Phys. Rev. C **99**, 014303 (2019)
151. A.J. Koning, S. Hilaire, S. Goriely, Nucl. Phys. A **810**, 13 (2008)
152. J. Holmes, S. Woosley, W. Fowler, B. Zimmerman, At. Data Nucl. Data Tables **18**, 305 (1976)
153. A. Coc, S. Goriely, Y. Xu, M. Saimpert, E. Vangioni, Astrophys. J. **744**, 158 (2012)
154. P.D. Group, P. Zyla, R. Barnett, J. Beringer, O. Dahl, D. Dwyer, D. Groom, C.J. Lin, K. Lugovsky, E. Pianori et al., Prog. Theor. Exp. Phys. **2020**, 083C01 (2020)
155. A. Aab et al. [Pierre Auger Collaboration], Phys. Rev. D **90**, 122005 (2014)
156. A. Aab, P. Abreu, M. Aglietta, J.M. Albury, I. Allekotte, A. Almela, J.A. Castillo, J. Alvarez-Muñiz, R.A. Batista, G.A. Anastasi et al., Phys. Rev. Lett. **125**, 121106 (2020)
157. N. Nagano et al., Nucl. Part. Phys. **18**, 423 (1992)
158. H.R.F.E. Collaboration, R. Abbasi, T. Abu-Zayyad, M. Allen, J. Amman, G. Archbold, K. Belov, J. Belz, S.B. Zvi, D. Bergman et al., Phys. Rev. Lett. **100**, 101101 (2008)
159. J. Abraham et al. [Pierre Auger Collaboration], Nucl. Instrum. Methods Phys. Res. A **523**, 50 (2004)
160. H. Tokuno et al., J. Phys. Conf. Ser. **293**, 012035 (2011)
161. P. Sokolsky, G.B. Thomson, J. Phys. G **34**, 401 (2007)
162. J. Abraham et al. [Pierre Auger Collaboration], Phys. Rev. Lett. **101**, 61101 (2008)
163. T. Abu-Zayyad, R. Aida, M. Allen, R. Anderson, R. Azuma, E. Barcikowski, J. Belz, D. Bergman, S. Blake, R. Cady et al. [Telescope Array Collaboration], Astrophys. J. Lett. **768**, L1 (2013)
164. R. Abbasi, M. Abe, T. Abu-Zayyad, M. Allen, R. Azuma, E. Barcikowski, J. Belz, D. Bergman, S. Blake, R. Cady et al. [Telescope Array Collaboration], Astropart. Phys. **80**, 131 (2016)
165. J. Abraham et al. [Pierre Auger Collaboration], Phys. Rev. Lett. **104**, 91101 (2010)
166. A. Aab et al. [Pierre Auger Collaboration], Phys. Rev. D **90**, 122006 (2014)
167. A. Aab, P. Abreu, M. Aglietta, I. Al Samarai, I. Albuquerque, I. Allekotte, A. Almela, J.A. Castillo, J. Alvarez-Muñiz, G.A. Anastasi et al., Science **357**, 1266 (2017)
168. A. Aab et al. [Pierre Auger Collaboration], Astrophys. J. **804**, 15 (2015)
169. P. Tinyakov et al. [Telescope Array Collaboration], TA anisotropy summary, in Proc. 34th ICRC, The Hague, The Netherlands (2015)
170. K. Greisen, Phys. Rev. Lett. **748**, 16 (1966)
171. G.T. Zatsepin, V.A. Kuzmin, JETP Lett. **4**, 78 (1966)
172. E. Khan et al., Astropart. Phys. **23**, 191 (2005)
173. J.L. Puget, F.W. Stecker, J.H. Bredekamp, Astrophys. J. **205**, 638 (1976)
174. E. Kido, T. Inakura, M. Kimura, N. Kobayashi, S. Nagataki, N. Shimizu, A. Tamii, Y. Utsuno, (2022). arXiv: 2206.03447 [astro-ph.HE]
175. T. Inakura, T. Nakatsukasa, K. Yabana, Phys. Rev. C **80**, 044301 (2009)
176. P.L. Biermann, P.A. Strittmatter, Astrophys. J. **322**, 643 (1987)
177. J.P. Rachen, P.L. Biermann, A&A **272**, 161 (1993). arXiv:astro-ph/9301010
178. M.R. George, A.C. Fabian, W.H. Baumgartner, R.F. Mushotzky, J. Tueller, MNRAS **388**, L59 (2008). arXiv:0805.2053
179. F. Fraschetti, F. Melia, MNRAS **391**, 1100 (2008). arXiv:0809.3686
180. H. Takami, S. Horiuchi, Astropart. Phys. **34**, 749 (2011). arXiv:1010.2788
181. J.H. Matthews, A.R. Bell, K.M. Blundell, A.T. Araudo, MNRAS **482**, 4303 (2019). arXiv:1810.12350
182. E. Waxman, Phys. Rev. Lett. **75**, 386 (1995). arXiv:astro-ph/9505082
183. E. Waxman, Astrophys. J. **452**, L1 (1995). arXiv:astro-ph/9508037
184. M. Vietri, D. De Marco, D. Guetta, Astrophys. J. **592**, 378 (2003). arXiv:astro-ph/0302144
185. B.D. Metzger, D. Giannios, S. Horiuchi, MNRAS **415**, 2495 (2011). arXiv:1101.4019
186. L.A. Anchordoqui, G.E. Romero, J.A. Combi, Phys. Rev. D **60**, 103001 (1999). arXiv:astro-ph/9903145
187. L.A. Anchordoqui, Phys. Rev. D**97**, 063010 (2018). arXiv:1801.07170
188. E. Peretti, G. Morlino, P. Blasi, P. Cristofari, MNRAS **511**, 1336 (2022). arXiv:2104.10978
189. H. Kang, D. Ryu, T.W. Jones, Astrophys. J. **456**, 422 (1996). arXiv:astro-ph/9507113
190. P. Blasi, A.V. Olinto, Phys. Rev. D**59**, 023001 (1998). arXiv:astro-ph/9806264
191. J. Kim, D. Ryu, H. Kang, S. Kim, S.C. Rey, Sci. Adv. **5**, eaau8227 (2019). arXiv:1901.00627

192. B.T. Zhang, K. Murase, F. Oikonomou, Z. Li, Phys. Rev. D **96**, 063007 (2017). arXiv:1706.00391
193. M. Arnould, S. Goriely, Prog. Part. Nucl. Phys. **112**, 103766 (2020)
194. C. Iliadis, Nuclear Physics of Stars, 2nd edn. (Wiley-VCH, 2015)
195. M. Arnould, S. Goriely, Phys. Rep. **384**, 1 (2003)
196. M. Arnould, S. Goriely, K. Takahashi, Phys. Rep. **450**, 97 (2007)
197. H. Utsunomiya, S. Katayama, I. Gheorghe, S. Imai, H. Yamaguchi, D. Kahl, Y. Sakaguchi, T. Shima, K. Takahisa, S. Miyamoto, Phys. Rev. C **92**, 064323 (2015)
198. C. Segebade, V.N. Starovoitova, T. Borgwardt, D. Wells, J. Radioanal. Nucl. Chem. **312**, 443 (2017)
199. S.R. Ibrahim, M. Musthafa, C. Midhun, S.L. Cyriac, S. Sajeev (2020)
200. F. Mirani, D. Calzolari, A. Formenti, M. Passoni, Commun. Phys. **4**, 1 (2021)
201. H. Toyokawa, H. Ohgaki, T. Hayakawa, T. Kii, T. Shizuma, R. Hajima, N. Kikuzawa, K. Masuda, F. Kitatani, H. Harada, Jpn. J. Appl. Phys. **50**, 100209 (2011)
202. M. Johnson, J. Hall, D. McNabb, J. McFarland, E. Norman, W. Bertozzi, S. Korbly, R. Ledoux, W. Park, Tech. rep., Lawrence Livermore National Lab. (LLNL), Livermore (2010)
203. J. Jones, B. Blackburn, S. Watson, D. Norman, A. Hunt, Nucl. Instrum. Methods Phys. Res. B **261**, 326 (2007)
204. S. Verbitskii, V. Emokhonov, A. Lapik, V. Nedorezov, A. Rusakov, G. Solodukhov, M. Tikhanov, A. Turinge, A. Tselebrovskii, Bull. Russ. Acad. Sci. Phys. **75**, 1544 (2011)
205. J. McFee, A. Faust, K. Pastor, Nucl. Instrum. Methods Phys. Res. A **704**, 131 (2013)
206. D. Habs, U. Köster, Appl. Phys. B **103**, 501 (2011)
207. T. Enoto, Y. Wada, Y. Furuta, K. Nakazawa, T. Yuasa, K. Okuda, K. Makishima, M. Sato, Y. Sato, T. Nakano et al., Nature **551**, 481 (2017)
208. Y. Wada, T. Enoto, K. Nakazawa, Y. Furuta, T. Yuasa, Y. Nakamura, T. Morimoto, T. Matsumoto, K. Makishima, H. Tsuchiya, Phys. Rev. Lett. **123**, 061103 (2019)
209. H. Utsunomiya, S. Goriely, M. Kimura, N. Shimizu, Y. Utsuno, G. Tveten, T. Renström, T. Ari-izumi, S. Miyamoto, Phys. Rev. C (2022)